Available on CMS information server **CMS IN 2007/012**

CMS Internal Note

The content of this note is intended for CMS internal use and distribution only

February 14, 2007

Optical Survey Analysis of the CMS Forward Pixel Detector and Application to Alignment with Tracks

A.V. Gritsan, N. Tran

Johns Hopkins University, Baltimore, Maryland, USA

M. Kubantsev

Northwestern University, Evanston, Illinois, USA

Abstract

Analysis of the sensor positions within the CMS Forward Pixel Detector (FPD) is presented. Optical survey of the FPD panels and disks shows displacements from nominal geometry of order $\sim$100μm. Developed tools of 3D sensor position analysis allow us to extract the error matrix of the panel survey measurements which giving us precision of about $\sim$0.5μm in sensor plane and $\sim$2μm out of plane. The errors are larger for bigger structures as preliminary results of the full FPD survey indicate. We suggest to integrate these survey analysis results into the procedure of software alignment with tracks. The detailed χ^2 method is proposed and tested.

Contents

1 Introduction

The all-silicon design of the CMS tracker is well suited for high resolution measurements of tracks of particles. It also poses challenges in the calibration of the position of all the sensors after the hardware assembly is completed. Understanding the alignment of thousands of silicon sensors is necessary to a micron precision and becomes the decisive factor in success of the program.

Given the inaccessibility of the interaction region, it is impossible to measure the detector positions using conventional survey techniques once the detector has been installed. The only accurate way to determine the silicon detector positions is to use the data generated by the silicon detectors when they are traversed in-situ by charged particles. However, the so-called software alignment with information from tracks is complex and has difficulty in constraining all the spatial degrees of freedom with either a limited number of tracks (in the initial stages of experiment) or with poor connection between different pieces of the detector with charged-particle tracks. In the initial stages of the experiment the convergence of the software alignment with tracks could be improved if prior optical survey measurements are used for the initial track reconstruction. However, this optical survey information will be lost in subsequent track reconstruction if survey measurements are used only as initial values for alignment parameters.

In this note we study precision of sensor placement using example of the CMS Forward Pixel Detector (FPD) and its survey at Fermilab, analyze survey data to reconstruct the initial alignment of the detector components, like sensors, panels, half disks and half cylinders. We propose to implement the new procedure of including optical survey information as a constrain in the software detector alignment with tracks. The latter procedure provides orthogonal information to the software alignment with tracks and makes the procedure systematically more stable and robust.

2 Optical Survey of Forward Pixel Panels

For initial tests, we use optical survey measurements of two prototype panels (A01 and A02) completed at Fermilab between January and May 2006. Positions of four fiducial points [1] and four sensor corners have been measured for each sensor on a panel (three sensors correspond to 2×3, 2×4, and 2×5 plaquettes). Fig. 1 illustrates the panel and fiducial points used. Other features on the panel have been surveyed as well, but are not used in this study because of poor precision of their position with respect to the sensors. We also find that sensor corners do not provide precise reference system and for sensor alignment we use only fiducial point measurements.

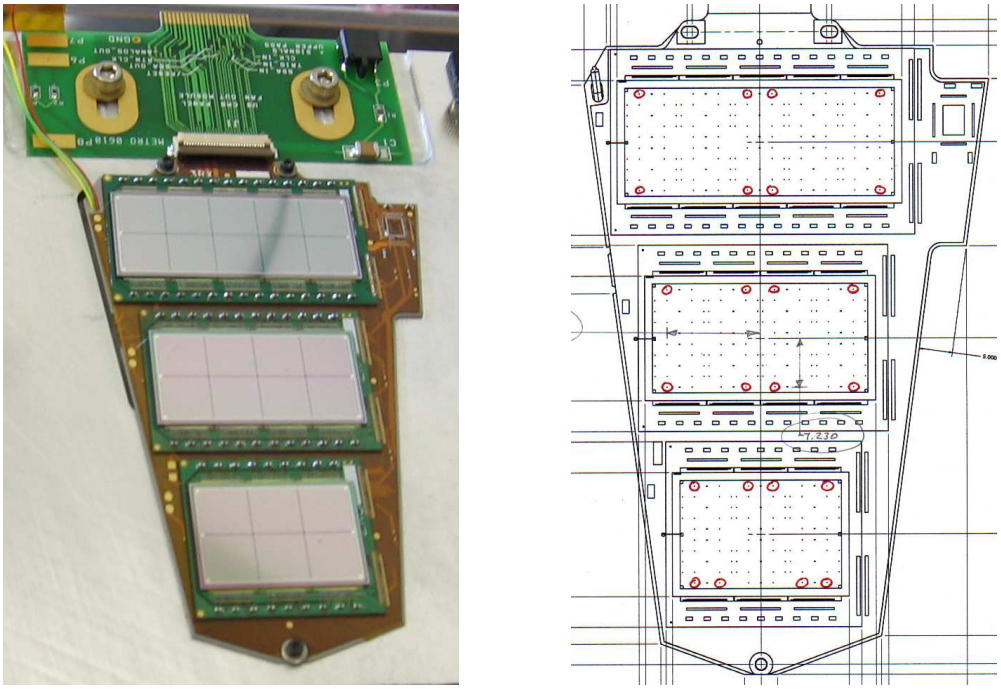

Figure 1: *Left: first forward pixel panel (three-sensor configuration); right: drawing of fiducial points on a panel.*

Afterwards, we use optical survey measurements [2] of the first 53 production panels recently completed at Fermilab. In addition, we also use optical survey measurements of four mechanical panels whose results we need for the half disk survey mentioned later (A02, A01L, XA01, X0004). The prefix P3R refers to a three-sensor panel (corresponding to 2×3, 2×4, and 2×5 plaquettes) with right-handed orientation. The prefix P4R refers to a four-sensor panel (corresponding to 1×2, 2×3, 2×4, and 1×5 plaquettes) with right-handed orientation. Positions of eight fiducial points have been measured for each sensor on each assembled panel [3]. [3] also gives the coordinate system in which the sensor displacements are presented.

Initially, we use a stand-alone application based on Root data-analysis framework [4] to perform our analysis, but later move to an application integrated into CMSSW. The advantage of implementation in CMSSW is that we are able to use the ideal geometry database within the software which will help with surveys of higher level detector components with more complicated nominal geometries. As an example, the next section deals with initial optical survey of the half disk. Results of the two applications were verified to be in agreement with each other with accuracy much better than present survey errors.

2.1 Sensor Displacements

We work out transformations (translation $\vec{R}$ and rotation $\vec{\Omega}$) which bring the measured and reference panel into one aligned system. As an example, the values of $\vec{R}$ and $\vec{\Omega}$ can found in the formalism of rigid body motion which we adopt to our task, see Eq. (1) and (2):

$$(\sum_{j,i}^{n\times N} m_{ij})R_k = (\sum_{j,i}^{n\times N} m_{ij} \cdot d\vec{r}_{ij})_k \tag{1}$$

$$\sum_{k=1}^{3} \Omega_k \sum_{j,i}^{n\times N} m_{ij}(\delta_{kl}(\vec{r}_{ij})^2 - (\vec{r}_{ij})_k(\vec{r}_{ij})_l) = \sum_{j,i}^{n\times N} m_{ij}(\vec{r}_{ij} \times d\vec{r}_{ij})_l \tag{2}$$

Here we have $N = 3$ or 4 sensors per panel with $n = 8$ fiducial points measured for each sensor on each production panel. The relative "mass" of each point m_{ij} is effectively the weight of each measurement and is set to be equal for all points. The relative displacements $d\vec{r}_{ij}$ (between survey and reference sets) and global positions $\vec{r}_{ij}$ of each point are used in the calculation. After the global transformation $\vec{R}$ and $\vec{\Omega}$, we effectively overlay the survey measurement on the reference system of the panel.

After the measured and reference panels are aligned, we find transformation of each sensor (translation $\vec{R}_i$ and rotation $\vec{\Omega}_i$). We apply the same formalism in Eq. (1) and (2) with i fixed to a particular sensor instead of sum over N sensors. We illustrate these results in Fig. 2 for two production panels, P3R-001 and P4R-001, respectively. Appendix. A shows visualizations of all of the production panels to date. The relative displacements and rotations are magnified by 20. In Table 5 located in Appendix A , we provide numerical values of the sensor displacements for three-sensor and four-sensor production panels, respectively. In both displacement tables, we also add sensor displacements for the mechanical panels whose results are needed later. From Table 5 and Appendix. A, we note that the P4R panels are more greatly misaligned than the P3R panels.

In Fig. 3, we compare the sensor displacements for prototype panel A02 from January and May which confirms good agreement between measurements done at different times.

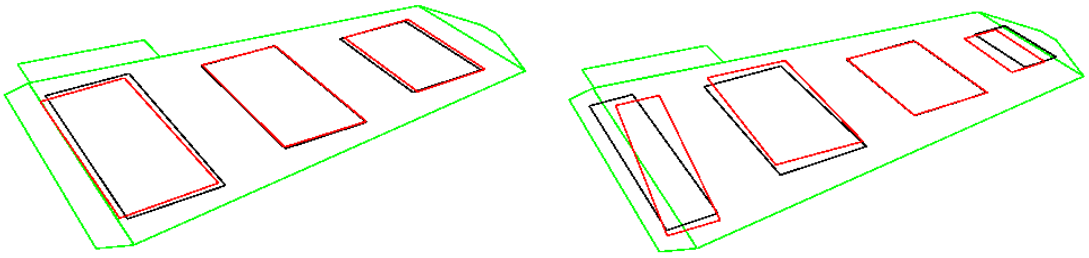

Figure 2: *Comparison of the relative sensor positions with the nominal and measured alignment parameters for one three-sensor panel and one four-sensor panel. The relative displacements and rotations are magnified by 20.*

To illustrate another measure of the displacement of the sensors, we compare the distributions of fiducial point displacements between the survey measurements and the reference positions after the two sets of measurements are aligned with the global transformation discussed above. This is shown in Fig. 4. The typical displacements are in agreement with numbers in Table 5 in Appendix A

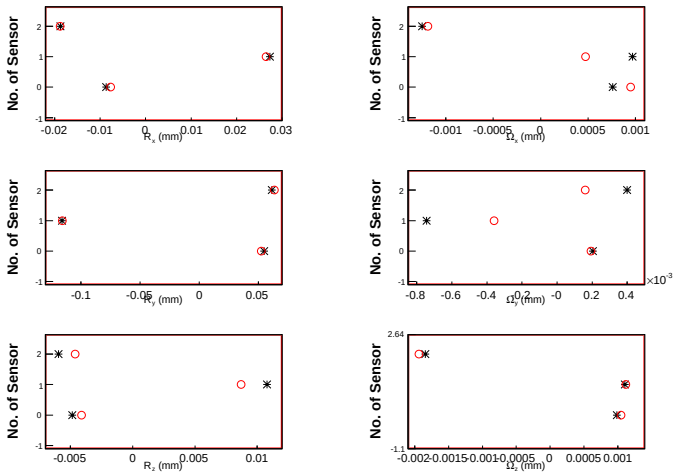

Figure 3: *Comparison of the sensor displacements for panel A02 from January and May. Displacement measures in left (in mm): R_x (top), R_y (middle), R_z (bottom); right (in radian): Ω_x (top), Ω_y (middle), and Ω_z (bottom) Stars represent January data and circles represent May data. Sensor 0 is 2x3; sensor 1 is 2x4; sensor2 is 2x5.*

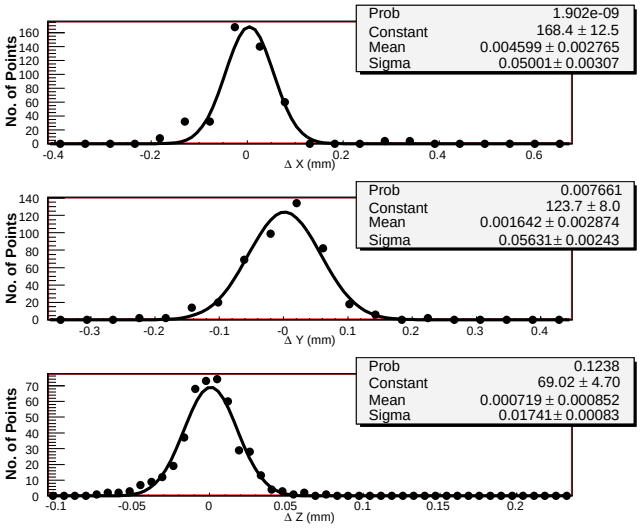

Figure 4: *A distribution of displacement of individual points for the first 25 production panels in the x, y, and z-directions with respect to the nominal geometry (given in Table 5). They are labeled as ΔX, ΔY, and ΔZ, respectively.*

2.2 Error in Optical Survey

By transforming each sensor by the values found in Table 5, we perform a cross-check to determine the error in the actual measurements determined by the optical survey. These results are shown in Fig. 5. The typical disagreement is less than 0.5 μm in x and y, and at the order of 2 μm in z. These numbers represent the typical errors in the survey measurements or distortions of the sensor geometry from ideal flat shape. These numbers might be slightly optimistic due to global position adjustment, but they set the scale on the errors.

Further analysis of measurement error was done via simulation. Assuming a measurement error of 1 μm in the x and y-directions and a measurement error of 5 μm in the z-direction, we analyze how such errors would manifest

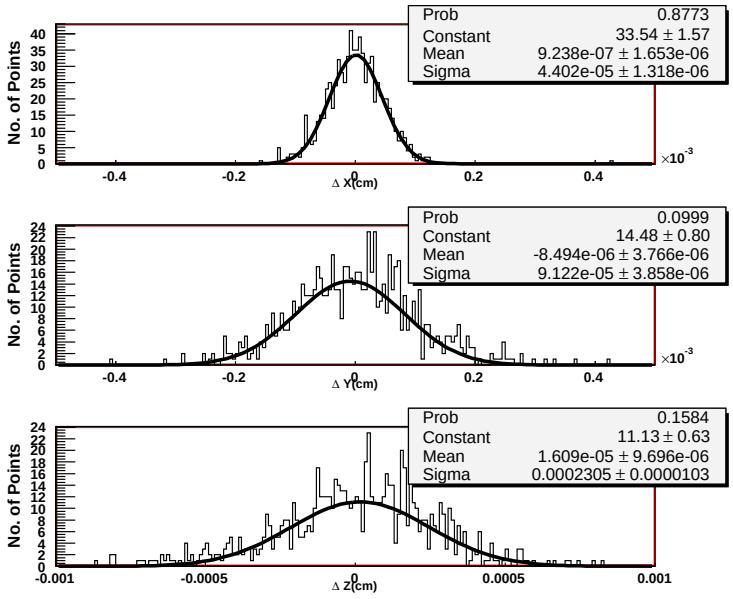

Figure 5: *A distribution of displacement of individual points in the x, y, and z-directions after transformation by displacement of measured sensor positions with respect to the nominal geometry. They are labeled as ΔX, ΔY, and ΔZ, respectively.*

themselves in the previous error analysis. The errors were implemented by taking a random Gaussian distribution about the nominal point with a σ in the x, y, and z-directions indicated above. The simulation was done for 100 panels; Fig. 6 is analogous to actual data in Fig. 5. We see from Fig. 6 that the error in the distribution is in agreement with the assumed measurement error.

As a further analysis, we explore how errors in the measurement of individual points would manifest themselves in values of the transformation vectors. With the same 100 simulated panels, we determine the translation and rotation vectors associated with the assumed measurement error for each sensor. These are plotted in Fig. 7. The error from the distributions for the transformation vectors are less than the measurement errors, they roughly scale as $1/\sqrt{n}$ in x, y, and z for n fiducial points per sensor. For R_x and R_y, the error is approximately 0.4 μm, and for R_z, the error is approximately 1.9 μm. We understand these to be an error for the values in Table 5. assuming the measurement error of 1 μm in the x and y-directions and a measurement error of 5 μm in the z-direction.

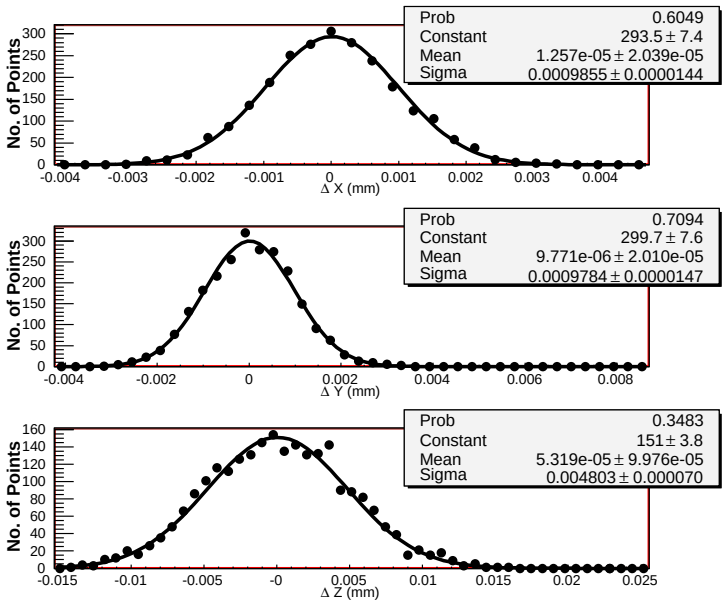

Figure 6: *A distribution of displacement of individual points in the x, y, and z-directions with respect to the nominal points. This figure shows the distribution for 100 simulated panels with a measurement error of 1 μm in the x and y-directions and 5 μm in the z-direction. They are labeled as ΔX, ΔY, and ΔZ, respectively.*

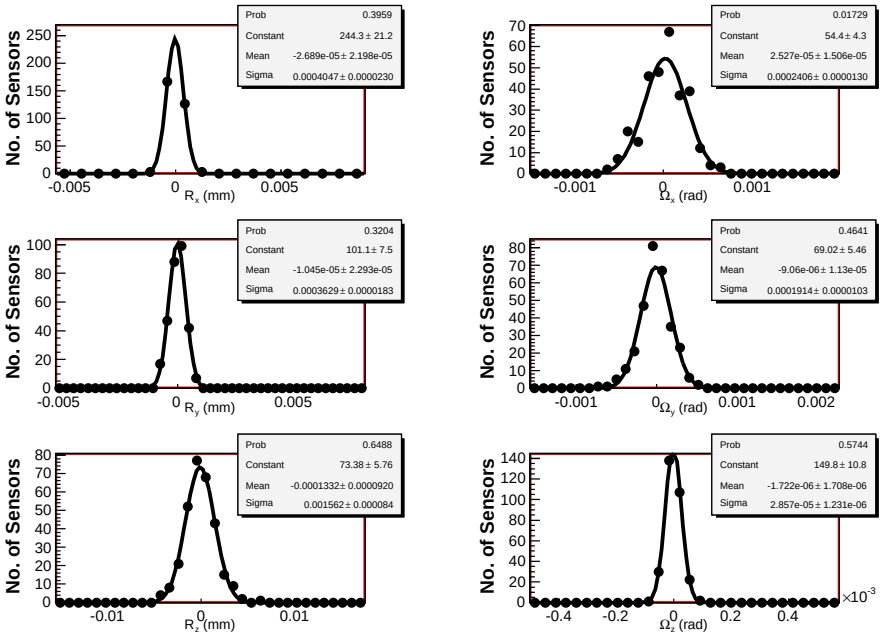

Figure 7: *For the 100 simulated panels, a distribution of the translation and rotation vectors for each sensor are plotted to understand what the effects would be from the measurement errors. Left column, top to bottom: R_x, R_y, R_z (mm); right column, top to bottom: Ω_x, Ω_y, Ω_z (radian).*

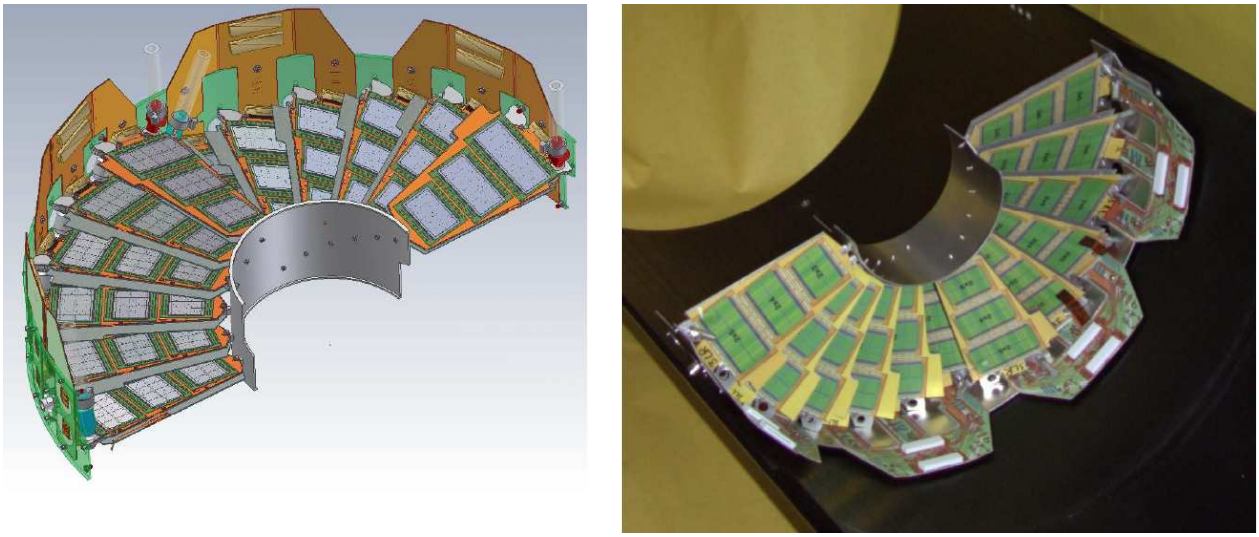

Figure 8: *Model of the forward pixel half-disk.*

3 Optical Survey of Forward Pixel Half Disk (one side only)

The next task is to perform the same sort of analysis on a half disk of the CMS Forward Pixel detector, see Fig. 8. For the analysis, we use the data from initial half disk surveys described in Ref. [6]. In this initial half disk survey, 3 three-sensor panels and 1 four-sensor panel are installed on the half disk and visible fiducial points are surveyed; mechanical panels A02, A01, XA01, and X0004 are the installed panels. We call this initial half disk survey the prototype half disk. Study of the error in the half disk study was done using this prototype half disk. In addition, we provide analysis of the two pilot run half disks, P1 and P2. For these half disks, 2 four-sensor and 2 three-sensor panels were install on each. The P1 half disk includes panels: P4R-020, P4R-001, P3R-001, P3R-002. The P2 half disk includes panels: P4R-036, P4R-005, P3R-003, P3R-004. Visualization of the positions of the panels is provided below.

There are a few new noteworthy features for this analysis. First, the 8 fiducial points per plaquette used in the panel surveys are not all visible in the half disk survey. This also presents a challenge in finding out exactly which fiducials are being used since there are 20 fiducial points per fiducial chip. Second, because of the growing complexity of the ideal geometry, the ideal geometry database within CMSSW was utilized. There were a few caveats between the optical survey measurements and the ideal geometry in CMSSW such as differing units (cm vs. mm) and the different local systems for sensors and panels. As mentioned before, the local system for sensors is given in [3]. The panel displacements are presented in the CMSSW local frame given in [5].

3.1 Panel Displacements Within One Side of a Half Disk

The analysis proceeded with the same rigid body motion formalism adopted for the forward pixel panel analysis. However, instead of finding sensor displacements within the panel, we found panel displacements within the half disk. The procedure was to generate a set of fiducial points based on the ideal geometry database corresponding to the points surveyed. To correct for the sensor distortions of each panel installed on the half disk, we shift the fiducial points on each relevant sensor by the appropriate amount determined from panel analysis. Then, we placed the measured half disk system onto our fiducial system and determined the panel translations and rotations. As mentioned before, the challenge of not having exactly 8 fiducial points per sensor complicated the analysis; the rigid body formalism is not always summed over $n = 8$ fiducial points in Eq. (1) and Eq. (2).

In Table 1, we provide the numerical values of the panel displacements for the three mechanical panels installed on the half disk for the prototype half disk. Since there was only one panel, X004, on the opposite side, we cannot present any panel displacement on the half disk for the four-sensor side. All numerical values are presented about the center of mass of the panels. This means that for the three-sensor panel, rotations and translations will be presented about the center of the 2×4 sensor; and for the four-sensor panel, rotations and translations will be presented about the point in between the 2×3 and 2×4 sensors. This will be especially relevant for four-plaquette panels since the center of mass of the panel is not located on a plaquette. In Table 1, we also give the panel

displacements for the P1 and P2 pilot run half disks. In Fig. 9, we illustrate panel displacements on the half disk for the prototype half disk. In Fig. 10, we illustrate panel displacements on the half disk for the P2 pilot run half disk. The positions of the panels illustrated in Fig. 10 are also the same locations for the P1 half disk.

Table 1: *Displacements of the measured panel positions with respect to the nominal geometry for inital half disk survey.*

half disk	panel	R_x (μm)	R_y (μm)	R_z (μm)	Ω_x (mrad)	Ω_y (mrad)	Ω_z (mrad)
prototype	XA01	22.8	-58.0	54.5	-0.26	1.81	-1.56
prototype	A01L	123.8	-73.9	-185.9	7.99	3.14	1.00
prototype	A02	-82.6	71.5	-7.1	4.98	2.06	5.03
P1	P4R-001	-44.2	12.2	8.8	2.25	1.29	-0.81
P1	P4R-020	84.5	-38.2	9.5	1.18	-0.71	-1.09
P1	P3R-002	-12.1	-38.1	14.1	-0.16	0.51	0.36
P1	P3R-001	-1.7	18.8	-12.4	1.28	-0.50	-0.77
P2	P4R-036	-14.0	-43.7	-35.4	-6.18	0.43	-0.94
P2	P4R-005	44.5	64.3	5.4	-1.71	-1.09	0.45
P2	P3R-003	15.3	-50.6	-66.7	5.47	1.31	0.06
P2	P3R-004	-12.5	20.2	-21.9	3.02	0.30	-0.06

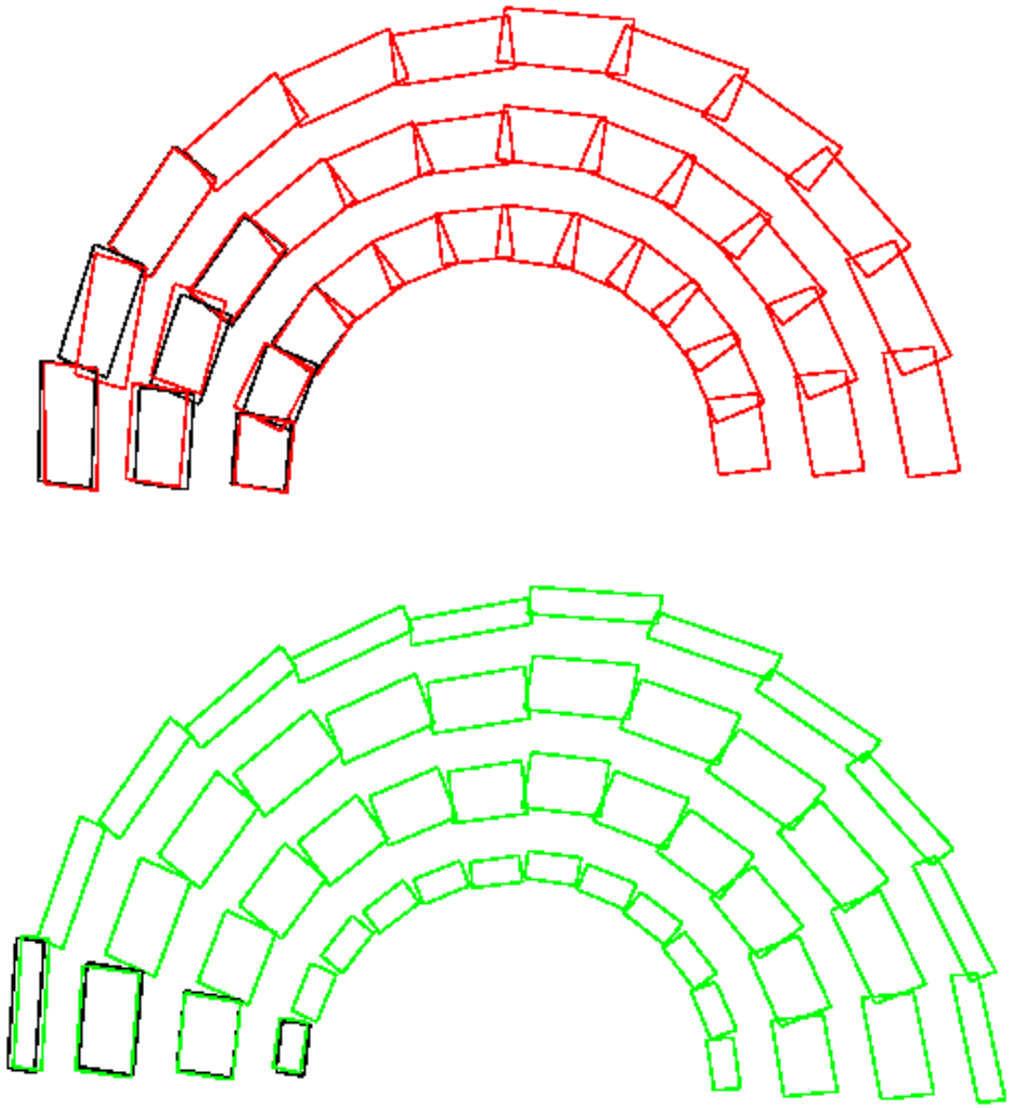

Figure 9: *Illustration of comparison between relative sensor positions with the nominal and measured alignment parameters for the initial half disk survey. Both sensor and panel displacements are displayed with a magnification factor of 20 both for displacements within the panel and the half disk(Top). For completeness, we illustrate a corresponding four-plaquette half disk (Bottom).*

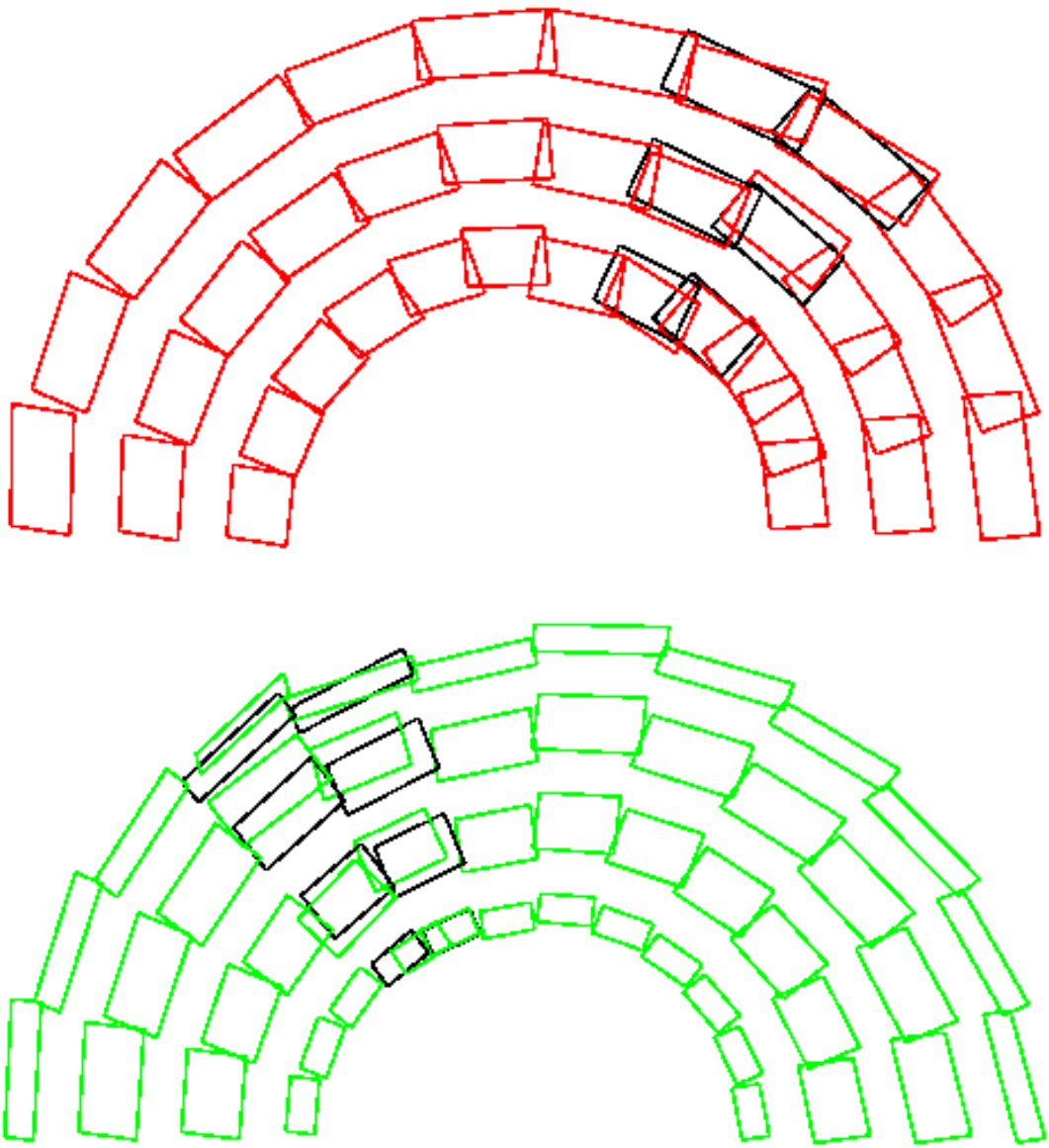

Figure 10: *Illustration of comparison between relative sensor positions with the nominal and measured alignment parameters for the P2 half disk survey. Both sensor and panel displacements are displayed with a magnification factor of 50.*

3.2 Error in Optical Survey of Half Disk

As was done in the panel survey, we transform each sensor by its panel displacement and each panel by its half disk displacement as a cross-check to determine the error in the actual measurements of the half disk survey. We plot the displacement of each point from the fiducial system in the x, y, and z-directions in Fig. 11. There were 38 points surveyed on the half disk: 20 from panel A02, 8 from panel A01L, and 10 from XA01. There are two points from panel A02 which do not lie within the expected geometry and cause ΔZ to have two strange points. These displacements are presented in the global ideal geometry system with the interaction point as the origin.

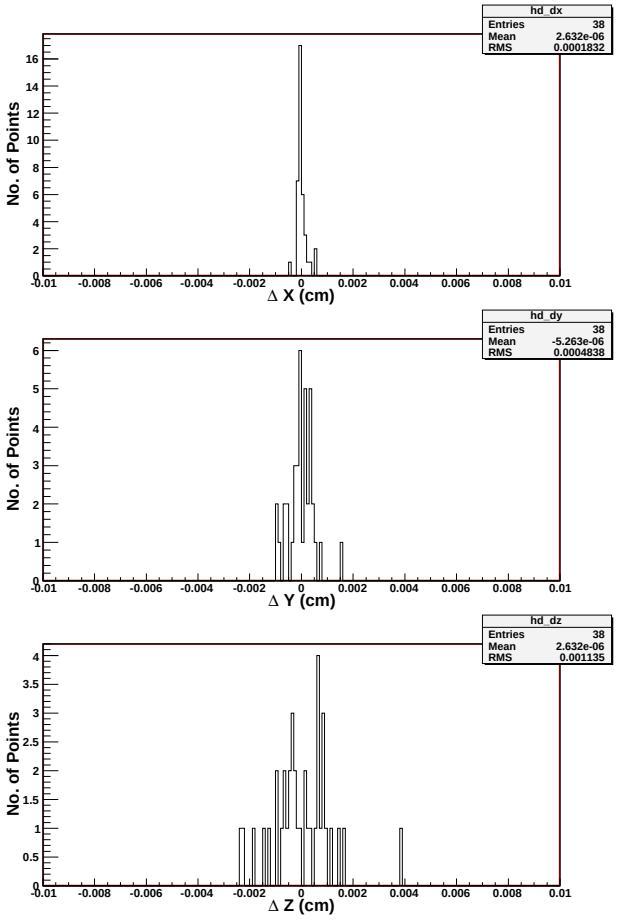

Figure 11: *A distribution of displacement of individual points in the half disk survey in the x, y, and z-directions with respect to the nominal points after transformation of points corresponding to both sensor and panel distortions.*

To further analyze the error associated with the half disk survey, we again run a toy Monte Carlo over 100 half disks. The further complication to this procedure which was different than error propagation in panel survey is that the number of survey points per panel can vary due to either poor visibility or poor measurement. For example, panel A02 from the three-plaquette side of the half disk had 20 visible fiducial points while panel A01 had only 8. The number of points is not the only factor in determining the error of measurements. In addition, the positions with which the points lay with respect to each other can also affect the error; for example, there is a difference between 4 point laying on a line and 4 points in a box-shape. Ultimately, there are many scenarios for which fiducial points will be surveyed, all with different associated errors. Thus, by attaching all panels to a half disk and seeing which fiducials are visible, a scenario can be generated for each panel and toy MC can be used to determined the error.

For illustrative purposes, we present two cases: 4 points on a panel all located on the same panel and 20 points on a panel as in panel A02. As was the case for previous toy MC analysis, we add random Gaussian values to each fiducial point and run our analysis. As was the case before, we associate a measurement error of 1 μm in the x and y-directions and a measurement error of 5 μm in the z-direction. Figure 12 and Figure 13 show a distribution of measurement errors per point for the 4-point and 20-point scenarios, respectively. Figure 14 and Figure 15

show how displacement of individual points are manifest in our translation and rotation vectors, $\vec{R}$ and $\vec{\Omega}$, for each panel. From these figures, we see that the more points used per panel give better precision for $\vec{R}$ and $\vec{\Omega}$, as we would expect.

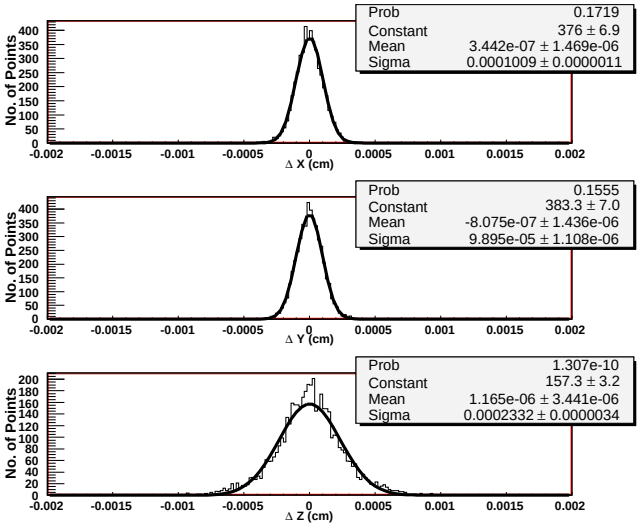

Figure 12: *Toy MC analysis of half disk survey for 4 points per panel. A distribution of displacement of individual points in the x, y, and z-directions with respect to the nominal geometry. They are labelled as ΔX, ΔY, and ΔZ, respectively.*

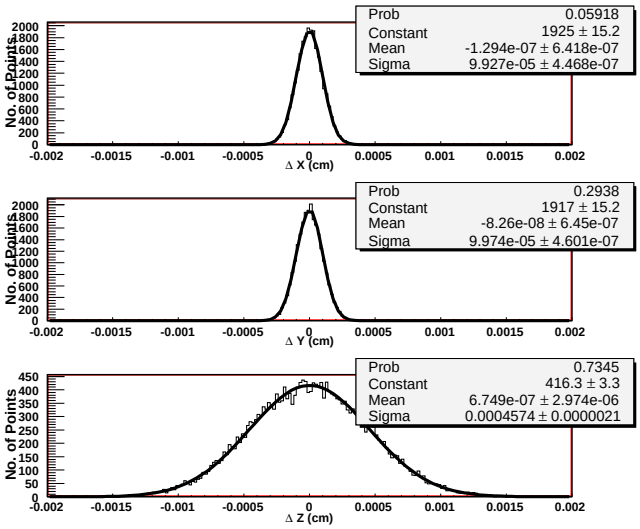

Figure 13: *Toy MC analysis of half disk survey for 20 points per panel. A distribution of displacement of individual points in the x, y, and z-directions with respect to the nominal geometry. They are labelled as ΔX, ΔY, and ΔZ, respectively.*

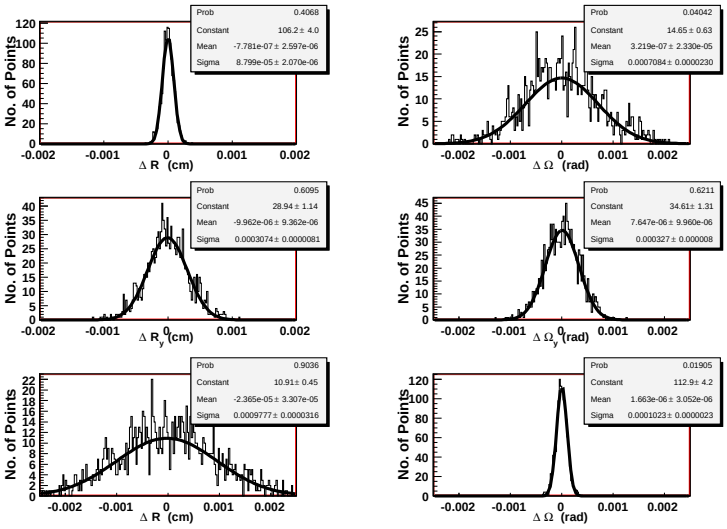

Figure 14: *Toy MC analysis of half disk survey for 4 points per panel. A distribution of translation and rotation vectors in the x, y, and z-directions with respect to the nominal geometry.*

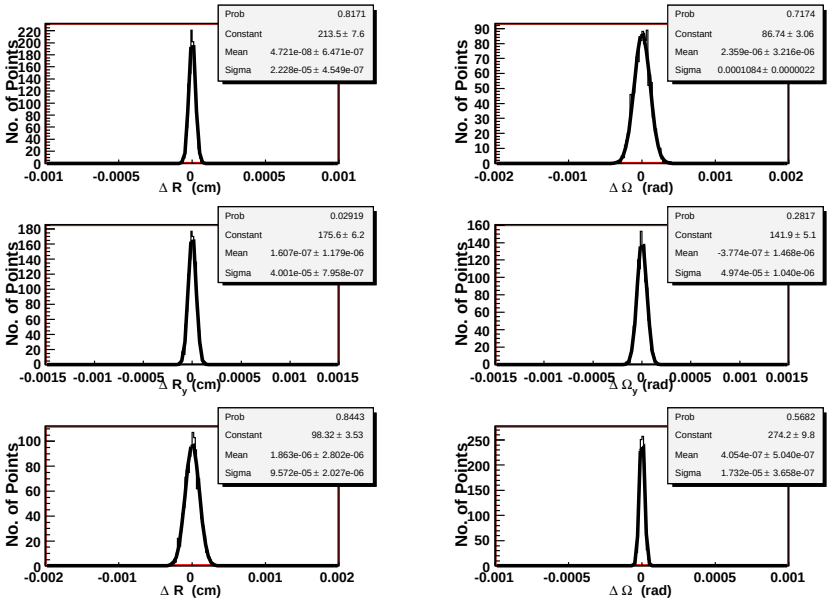

Figure 15: *Toy MC analysis of half disk survey for 20 points per panel. A distribution of translation and rotation vectors in the x, y, and z-directions with respect to the nominal geometry.*

4 Full Half Disk Survey Via Reference Targets

Our next goal is to create a full half disk from optical survey of two sides of a half disk, a three-plaquette side and a four-plaquette side. In doing so, we are able to create the blade structure. This is important because we expect the blade structure to be relatively stable in time once their positions have been established. Currently, there are two different procedures to combine the two sides of a full half disk. The first procedure uses ruby survey balls; the second procedure uses glass fiducials. Ruby survey balls can only be seen from one side of the half disk while the glass fiducials, located on the outside of the half disk support structure, are visible from both sides of the half disk. Thus, to combine the two sides of the half disk in the ruby survey ball procedure, it is necessary to take one more intermediate survey of all ruby balls without the panels installed on the half disk. This is illustrated in Fig. 16. A half disk has both types of reference balls, 5 ruby survey balls and 4 glass fiducials.

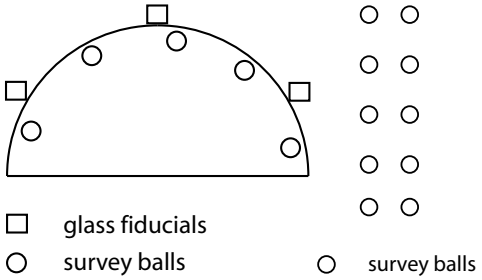

Figure 16: *Visualization of full half disk survey*

4.1 Ruby Survey Ball Method

The procedure to join two sides of a half disk uses rigid body formalism. The goal is to create a "measured system" of the full half disk consisting of only sensor fiducial points. In the survey ball method, we take the survey balls from the survey of one side of the half disk (i.e. 3-plaq side) and overlay them on their corresponding survey balls from the measurements which contains only survey balls without panels installed. We then do the same for the opposite side (i.e. 4-plaq side). In doing so, we also transform the sensor fiducials by the same values as the survey balls were overlayed. We illustrate this in Fig. 17. After creation of the measured full HD system, we overlay this

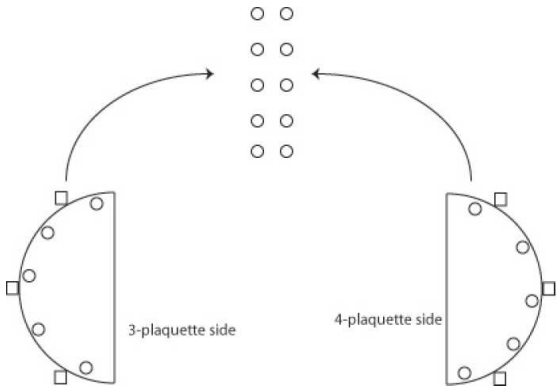

Figure 17: *Visualization of survey ball method*

on top of the ideal system from CMSSW and find corresponding displacements of the 3-plaq and 4-plaq sides.

4.2 Glass Fiducial Method

In order to create the measured full HD system in this case, there requires no intermediate overlaying of the glass fiducials because they are visible from both sides of the half disk. Here we simply lay the glass fiducials from one side (i.e. 4-plaq side) onto the corresponding glass fiducials from the other side (i.e. 3-plaq side). We illustrate this in Fig. 18. Then, as before, we overlay this measured system onto the ideal geometry and find displacements.

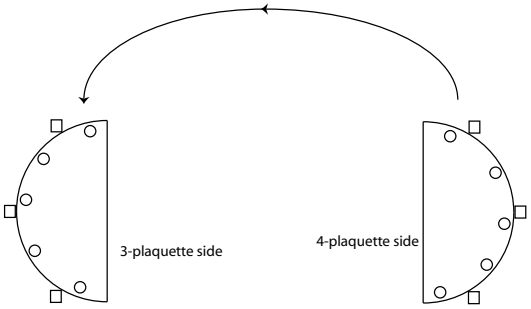

Figure 18: *Visualization of glass fiducial method*

4.3 Support Frame Analysis

Preliminary analysis of the two methods uncovered a possible discrepancy between the two methods. In an attempt to determine the source of any discrepancy between the two methods, we perform analysis of the reference targets themselves. In this study, 4 glass fiducials and 4 ruby survey balls were mounted onto a support frame and were measured from both sides. The procedure is to start with the measurements from the "three-sensor side" (ruby balls and glass fiducials) and overlay the corresponding ruby balls from the "four-sensor side". Then, we compare the positions of the glass fiducials from both sides. In Table 2, we give the difference in x, y, and z for each of the 8 reference points.

From this table, we see a $\sim 100\mu m$ shift in the z direction which may be attributed to parallax in the glass. The glass has an index of refraction of approximately ~ 1.5, and the thickness of the glass fiducials is $300\ \mu m$. From geometrical optics, we calculate the parallax effect to be $(n-1)/n\times$(thickness) $\sim 100\ \mu m$, which is the value we observe. We also see a $\sim 20\mu m$ shift in the x direction which is not accounted for, but we suspect may be due to some calibration issues between the touch probe and the optics which would cause an error in the ruby survey ball measurements.

Table 2: *Results from the analysis of the support frame survey. By overlaying the ruby balls on top of one another, we look for differences in the positions of the glass fiducials.*

reference target	$\Delta R_x\ (\mu m)$	$\Delta R_y\ (\mu m)$	$\Delta R_z\ (\mu m)$
Ruby 1	1.01	1.27	-0.004
Ruby 2	3.01	2.22	0.006
Ruby 3	-8.01	-4.01	-0.009
Ruby 4	3.99	0.52	0.007
Glass 1	-23.15	0.24	107.00
Glass 2	-22.15	2.21	100.01
Glass 3	-18.21	0.96	109.99
Glass 4	-9.21	2.52	110.01

Table 3: *Displacements of the measured half disk positions with respect to the nominal full half disk geometry as analyzed using the survey ball method. Translations are given in μm and Rotations are given in $mrad$.*

half disk	$\Delta R_x\ (\mu m)$	$\Delta R_y\ (\mu m)$	$\Delta R_z\ (\mu m)$	$\Delta\Omega_x\ (mrad)$	$\Delta\Omega_y\ (mrad)$	$\Delta\Omega_z\ (mrad)$
P1	160.4	59.1	-13.3	1.4	-0.1	-1.3
P2	62.5	3.5	145.0	0.41	-2.4	0.33

Table 4: *Displacements of the measured half disk positions with respect to the nominal full half disk geometry as analyzed using the glass fiducial method. Considered to be the final result. Translations are given in μm and Rotations are given in $mrad$.*

half disk	$\Delta R_x\ (\mu m)$	$\Delta R_y\ (\mu m)$	$\Delta R_z\ (\mu m)$	$\Delta\Omega_x\ (mrad)$	$\Delta\Omega_y\ (mrad)$	$\Delta\Omega_z\ (mrad)$
P1	85.1	10.7	-192.5	.04	-2.2	-0.86
P2	72.2	37.9	29.7	0.28	-3.5	0.19

4.4 Half Disk Displacements

Studies of both methods were conducted using the two pilot run half disks, P1 and P2. Here, we give results for the two different methods of combing the full half disk. The coordinate system for all results in the full half disk analysis are those used in the CMSSW ideal geometry (z is along the beam axis and x and y are in the plane of the half disks). At this time, the displacements are presented with respect to the center of mass of the points. In the future when using a more complete set of points, it may make sense to report displacements with respect to a central point such as the center of the half disk circle. Results are presented as the displacement of the four-plaquette side with respect to the three-plaquette side; more specifically, overlaying the three-plaquette side on the ideal geometry and measuring the displacement of the four-plaquette side. The results for the survey ball method are given in Table 3. One issue that complicates these results is the error in the ruby ball measurements due to overlay of the two systems. The error associated with this is approximately $\sim 20\ \mu m$. In addition, some of the measurements were taken at different times and it is a strong possibility that positions of ruby survey balls may have shifted over time and after re-installation of panels; there is also the issue of miscalibration between the touch probe and optics.

The results for the glass fiducial method are given in Table 4. These results account for the parallax, which is approximately $\sim 100\ \mu m$; we expect these results to be relatively stable. From the results given here, we still see a discrepancy between the two methods, but not outside of the errors of the ruby survey ball method. Considering the error in the ruby survey ball results, we consider the results from the glass fiducial method to be our final result.

4.5 Error in Half Disk Displacement

The source of error in the procedure to join two halves of a full half disk comes from how well we are able to match the survey balls on top of each other using the rigid body formalism. In Fig. 19, we show the displacement between measured survey balls on the half panel with and without the panels attached. On each side of the full half disk, there were only 3 stable survey balls; and these were the ones used to join the two sides. We see that the order of the error in the survey balls is on the order of the displacements of $\sim 10\ \mu m$; although, the z direction seems to have less of an error which is expected since the half disk structure would have less variance out of the plane of the half disk. This error about an order of magnitude less than the displacements themselves and agree with what is expected from the measurement of positions of survey balls.

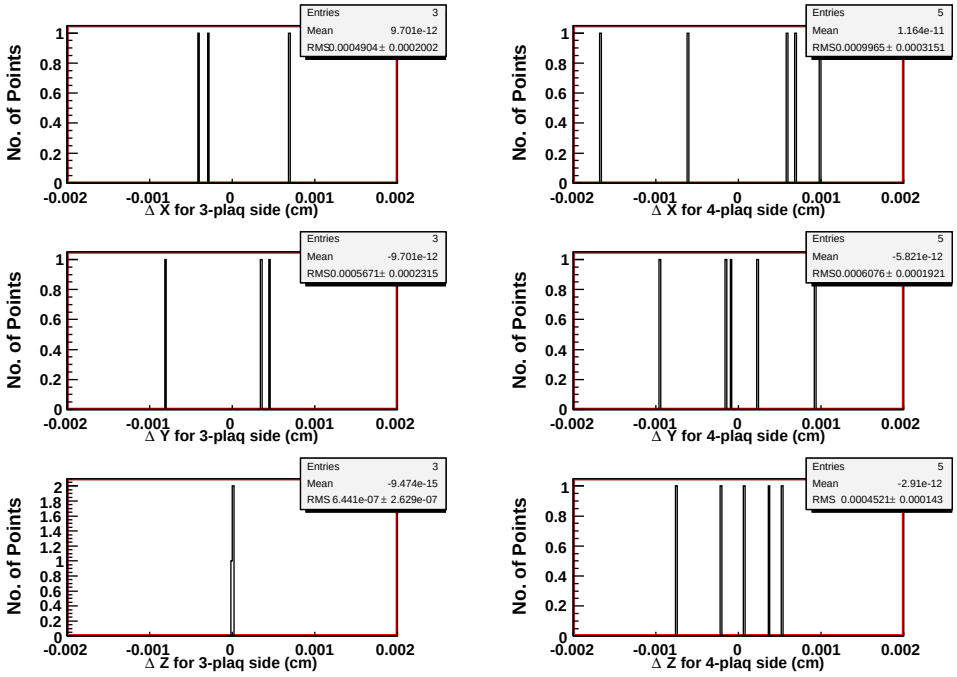

Figure 19: *The difference in position in the x, y, and z-directions between survey balls on the half disk with and without panels attached.*

As a further analysis of error in the full half disk survey, we use toy Monte Carlo to simulate how error in the ball

positions would be manifest in displacements of one side of the half disk. In a siumlation of 150 full half disks, we gave the survey balls a Gaussian distributed error of 10 μm in the x, y, and z-directions. We then run our analysis and determine the transformation of the half disks, R_{hd} and Ω_{hd}. For this simulation, we only used four survey balls, not all five, because this will be a more likely scenario. We understand R_{hd} and Ω_{hd} to be the errors given a 10 μm measurement error in the survey balls; they are given in Figure 20.

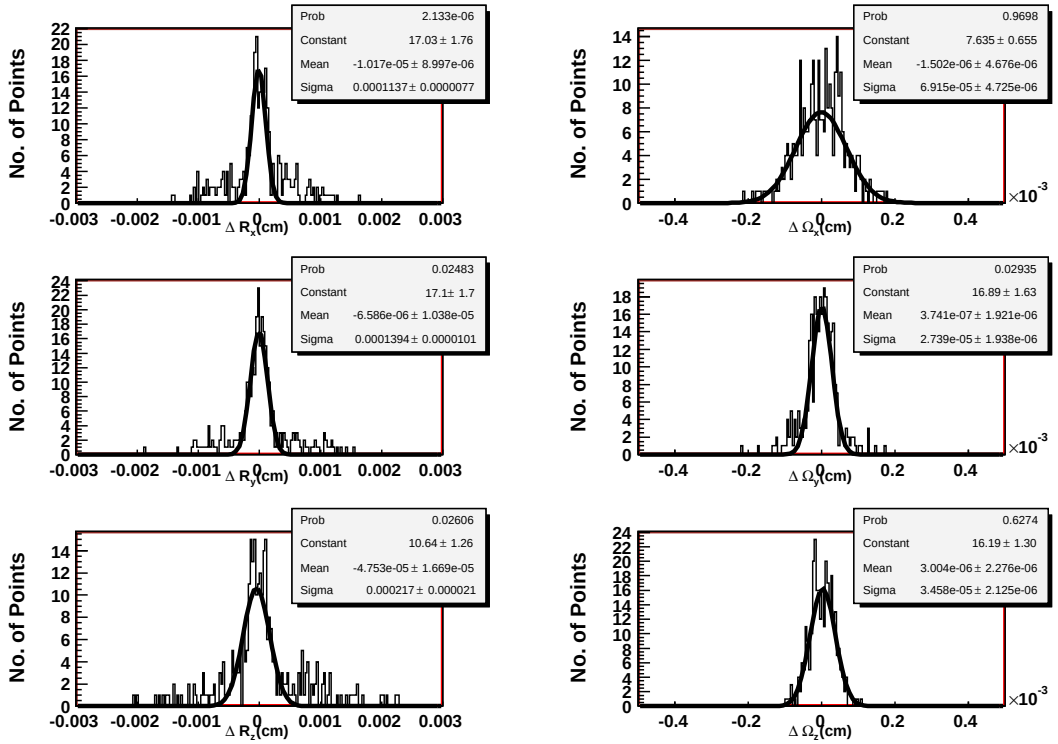

Figure 20: *A distribution of R_{hd} and Ω_{hd} for 150 simulated full half disks given a survey ball error of 10 μm for four survey balls.*

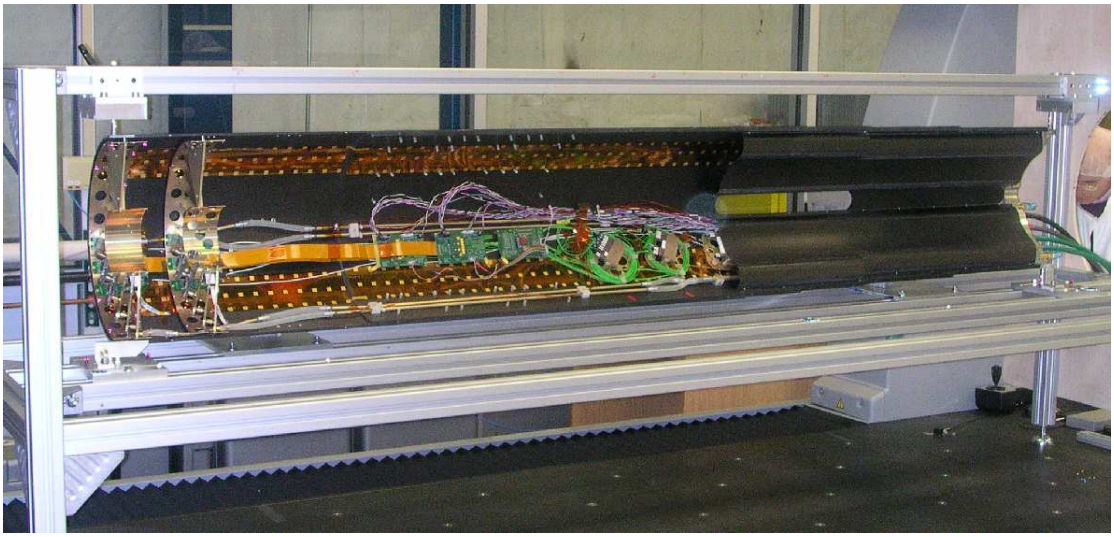

Figure 21: *Pilot Run (07) Forward Pixel half cylinder with two installed half disks during CMM and photogrammetry survey.*

5 Further Steps in Forward Pixel Detector Survey Analysis

There several other steps necessary in the optical survey analysis. First of all, we have to determine position of highr-level structures, such as half-disks, within the support structures. Second, we should be able to account for first-order correction in sensor position after the installation, such as due to temperature change and mechanical stress. These studies will be presented elsewhere, but we outline the main ideas below.

5.1 Half Disks Survey in the Service Cylinder

After the half disks are individually surveyed,they are mounted in pairs into a service half cylinder. Positions of these two half disks relative to each other and supporting structure are determined by two methods:

- First, using the CMM machine measuring survey balls on the half disks together with ones on the service cylinder and a support structure;
- Second, using photogrammetry of the optical targets and white survey balls.

Both methods are inter-calibrated using a big coordinate measuring machine (CMM) and photogrammetry at Fermilab. The picture of the 07 Pilot Run Forward Pixel half cylinder with two installed half disks during CMM and photogrammetry survey is shown in Fig. 21. The service half cylinder is mounted in the supporting frame substituting the rail system to be used in the CMS detector. The measurements with the CMM touch probe allow finding positions of the disks (including silicon sensors) relative to the precision balls on the supporting legs of the service cylinder standing on the frame.

At the same time set of photographs are made of these setup using a precise digital camera. Using these pictures, positions of a set of optical targets on the half disks, half cylinder and frame and the white survey balls on the frame are reconstructed using V-STARS photogrammetry software. Combining with CMM measurements of the survey balls two methods are connected and calibrated. The results of the 6-parameter fit of positions of these balls are presented in Fig. 22. Good agreement of order 10 microns is obtained.

After detector is moved to CERN we plan to make final photogrammetry survey during full detector assembly. Combination of these three measurements with data described above will allow full survey of the detector in working position.

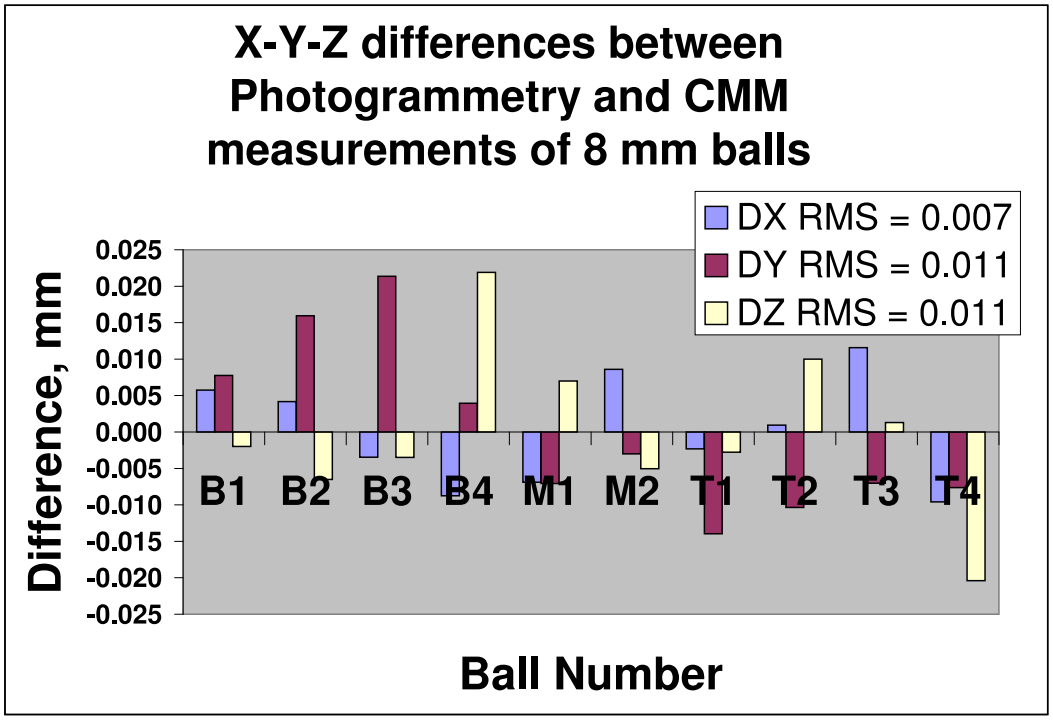

Figure 22: *Comparison of the CMM and photogrammetry measurements of the survey ball position on a test stand.*

5.2 Temperature Corrections for Survey Data

All the measurements described above are made at room temperature. Due to differences in CTE (a Coefficient of Thermal Expansion) relative positions of the silicon sensors mounted on the half disks at working temperature ($\sim -20^{\circ}$C) are changing by order of 100 microns. Since there is no internal alignment system to follow these variations inside the CMS detector we studied these effects using a mechanical model of the half disk with Beryllium panels and real cooling channel. The positions of the silicon targets on the panels were measured in temperature range of $+20^{\circ}$C to -20°C inside the cold box installed on the optical CMM. Final element analysis is used to describe these data and apply it to the final detector configuration. The results are to be presented elsewhere.

6 Application of the Optical Survey to Software Alignment

Modern silicon tracking detectors typically have a large number of measuring sensors, and statistical methods can be used to align individual sensors with respect to each other using tracks in-situ. For CMS there more than 20,000 sensors which need to be aligned. For an application of statistical methods to the CMS pixel detector, see for example Ref. [7]. These methods use the fact that the measured and trajectory impact points of a track are displaced if the sensor position is not known correctly, see Fig. 23. The required precision is a few μm, while installation precision is two or three orders of magnitude worse. This results in "residual" for each measurement i, which is generally a vector ϵ_i. One can minimize the χ^2 function which includes covariance matrix $\mathbf{V}$ of the measurement uncertainties:

$$\chi^2 = \sum_i \epsilon_i^T \mathbf{V}_i^{-1} \epsilon_i \tag{3}$$

The goal of the alignment procedure is to obtain six parameters for each independent sensor, these being the three spacial and three rotational parameters $(\mathbf{R}_j, \mathbf{\Omega}_j)$. In the above method the χ^2 could be minimized for each sensor separately and iterations could solve for correlations, or it could be minimized in one transformation which requires powerful computational techniques to account for correlations among many sensors.

While the methods for CMS silicon detector alignment with tracks are being developed, they do not envision using information about relative sensor position prior to installation, other than using them as the starting parameters in minimization algorithms. There is a hierarchical structure in the sensor assembly. Thermal and humidity effects and mechanical stresses make a detector move over time, so the relative position of higher-level structures may be somewhat unstable. However, relative positions of sensors within a panel or blade are expected to be stable.

We propose to include optical survey information in the full CMS detector alignment algorithm by extending the conventional χ^2 with tracks in Eq. (3) with an additional term, where for survey we sum over different structure constraints (e.g. $i =$ panel, blade, half-disk, etc):

$$\chi^2 = \sum_{i,\mathrm{track}} \epsilon_{i,\mathrm{track}}^T \mathbf{V}_{i,\mathrm{track}}^{-1} \epsilon_{i,\mathrm{track}} + \sum_{i,\mathrm{survey}} \epsilon_{i,\mathrm{survey}}^T \mathbf{V}_{i,\mathrm{survey}}^{-1} \epsilon_{i,\mathrm{survey}} \tag{4}$$

For example, for a half-disk CMS pixel structure we would have the following three terms in χ^2: sensor within a panel, blade, half-disk, see Eq. (5).

$$\chi^2_{\mathrm{survey}} = \epsilon_{\mathrm{p}}^T \mathbf{V}_{\mathrm{p}}^{-1} \epsilon_{\mathrm{p}} + \epsilon_{\mathrm{b}}^T \mathbf{V}_{\mathrm{b}}^{-1} \epsilon_{\mathrm{b}} + \epsilon_{\mathrm{hd}}^T \mathbf{V}_{\mathrm{hd}}^{-1} \epsilon_{\mathrm{hd}} \tag{5}$$

Minimization of χ^2 will allow us to obtain each sensor position $(\mathbf{R}_j, \mathbf{\Omega}_j)$. We start with a simple approach by writing down the full χ^2 term in Eq. (6).

$$\chi^2_{\mathrm{survey}} = \sum_{i=1}^{3} \left[\left[\sum_{j=1}^{3} \frac{(R_{i,j} - r_j)^2}{\sigma^2_{Ri,j}} \right] + \left[\sum_{j=1}^{3} \frac{(\Omega_{i,j} - \omega_j)^2}{\sigma^2_{\Omega i,j}} \right] \right] \tag{6}$$

Here, i is summed over the three levels of detector components: panel, blade, half-disk; and j is summed over the x, y, and z directions. The quantities $R_{i,j}$ and $\Omega_{i,j}$ are calculated from the rigid body formalism described above,

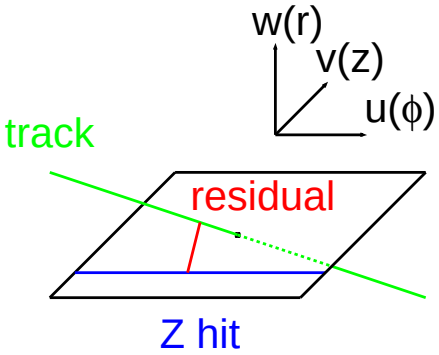

Figure 23: *Example of a silicon sensor with a charged track path displaced from the actual measurement ("hit").*

see Eq. (1) and (2). As an example, we minimize with respect to $\vec{r}$ and Eq. (8) yields the displacement vector from the χ^2 minimization procedure.

$$\frac{\partial \chi^2}{\partial \vec{r}} = 0 \tag{7}$$

$$\vec{r} = \sum_{j=x,y.z} \left[\frac{\sum_{i=1}^{3} \left(\frac{R_{i,j}}{\sigma^2_{Ri,j}} \right)}{\sum_{i=1}^{3} \left(\frac{1}{\sigma^2_{Ri,j}} \right)} \right] \hat{j} \tag{8}$$

Extension of the χ^2 for the joint use with the track residuals and the appropriate joint solution will be discussed elsewhere [8]. From the study of the optical survey measurements we propose to obtain a covariance matrix $\mathbf{V}_{\text{survey}}$ of the measurement uncertainties in the relative position of the sensors within a panel or the higher-level structures. The above proposed procedure can be naturally integrated into the existing alignment technique in Eq. (3) in the form of Eq. (4), and it has been successfully used in the past [9]. This procedure provides novel features:

- converges to the survey position using only a limited number of tracks in the beginning of experiment;
- constraints the relative position of sensors when only a poor connection through tracks exists;
- makes the procedure more robust when inevitable biases in the track reconstruction appear;
- allows us to adjust the weight of the survey measurements in the alignment algorithm;
- allows the survey position to change if more precise information is available from tracks;
- becomes the only constraint for “dead” read-out sensors, therefore preserving the geometry.

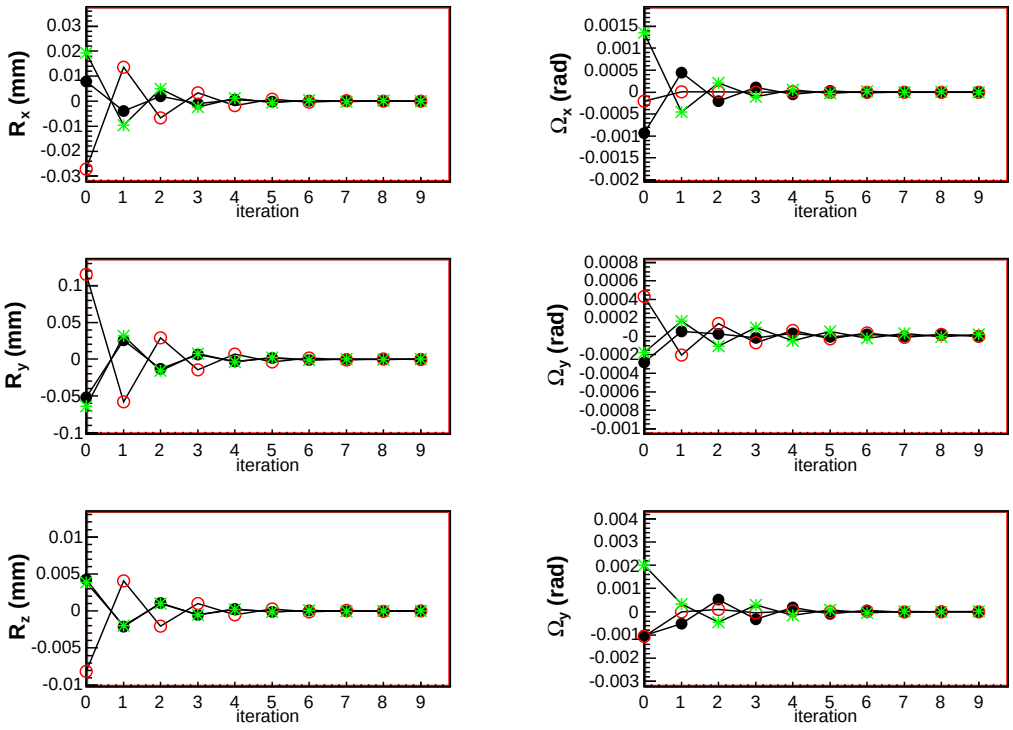

Figure 24: *Using sensor displacements from panel A02, a simulation of implementation of optical survey constraint in sensor alignment.*

6.1 Proof of Principle: Panel Alignment

We have performed a study of the optical survey constraint without presence of tracks. We simulated sensor displacements from panel A02 and allowed the algorithm to find the correct positions. Convergence of the algorithm to the right measured position is illustrated in Fig. 24.

6.2 Proof of Principle: Half Disk Alignment

As a more complex study, we simulate sensor displacement over an entire half disk, 84 sensors. We use χ^2 in Eq. (5) with the solution in Eq. (8), again using rigid body formalism in Eq. (1) and (2) to calculate residual R_i and Ω_i. In analogy with tracks, we calculate unbiased residuals, that is where the sensor in question does not affect the global shift of the reference unit prior to calculating residuals. We start with the ideal geometry and add Gaussian displacements of the typical order, $\sim 50\mu m$. Again, we see convergence to the correct position illustrated in Fig. 25.

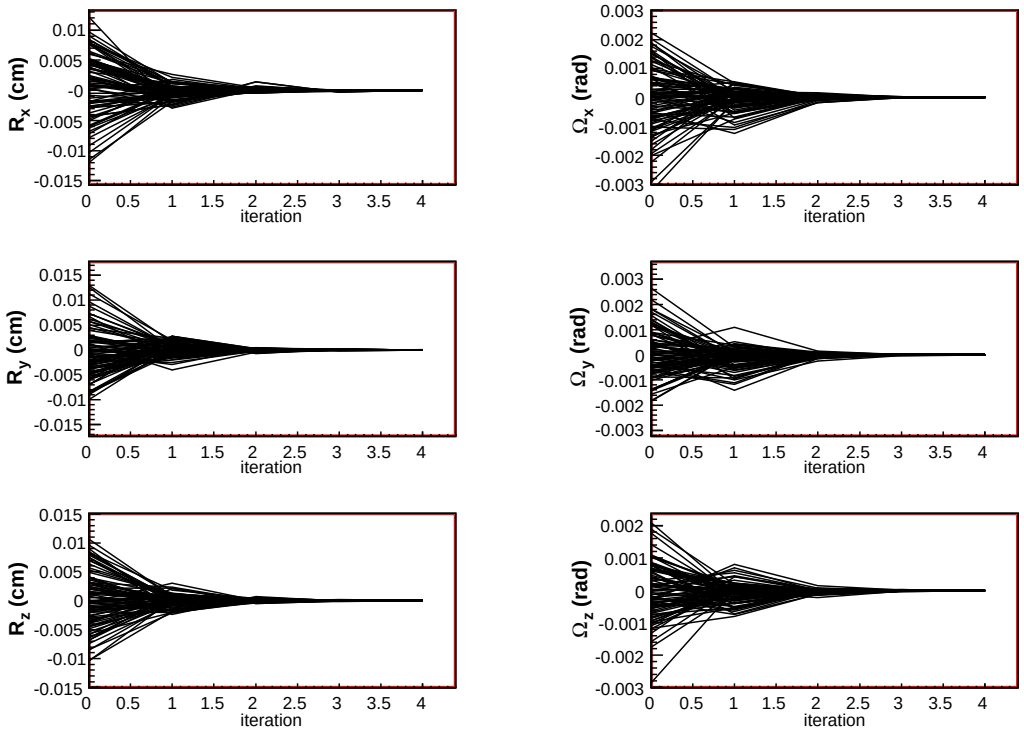

Figure 25: *Starting with ideal geometry and adding misalignments of the typical order, a simulation of implementation of optical survey constraint in sensor alignment.*

7 Summary

Discovery of new particles on CMS will depend on the ability to distinguish them from an enormous background of random particles produced in the high-energy collisions. Understanding the alignment of thousands of silicon sensors is necessary to a micron precision and becomes the decisive factor in success of the program. Imprecise knowledge of the sensor positions would result in low track reconstruction efficiency and low trigger efficiency, not to mention bad track parameter resolution, which would spoil the b-tagging and vertexing capabilities. This would make it impossible to measure the missing energy of the events or to tag the b-jets, which are believed to be the key signatures of new physics.

Study of the first optical survey results of the CMS forward pixel panels indicated sensor displacements from the nominal geometry of $\sim$100μm. We presented analysis of the sensor position within the CMS forward pixel panels. The developed tools of 3D sensor position analysis allowed us to extract error matrix of survey measurements, which is about $\sim$0.5μm in the sensor plane and $\sim$2μm out of plane. Study of the initial half disk optical survey found the panel displacements within the half disk to be $\sim$100μm. Further survey steps to align full FPD to the CMS coordinate system are outlined. We proposed to integrate the results of the optical survey analysis into the procedure of software alignment with tracks. The detailed χ^2 method has been proposed and tested with the examples of a panel or a half-disk. Some further details can be found in Ref.[8, 10].

A Displacements and Visualization of Panels

A.1 Panel Displacements

Table 5: *Displacements of the measured sensor positions with respect to the nominal panel geometry for all production panels and prototype panels (continues onto subsequent pages).*

panel	sensor	R_x (μm)	R_y (μm)	R_z (μm)	Ω_x (mrad)	Ω_y (mrad)	Ω_z (mrad)
P3L-002	2×3	22.8	35.1	-1.7	-0.07	0.03	4.90
	2×4	-11.3	28.6	3.7	-0.26	0.13	0.25
	2×5	-11.4	-63.7	-2.1	0.10	-0.09	1.90
P3R-001	2×3	-5.6	56.5	-7.1	-0.45	-0.40	0.38
	2×4	8.7	-1.2	10.9	0.14	-0.50	-0.57
	2×5	-3.1	-55.3	-3.8	2.13	0.45	-0.13
P3R-002	2×3	-22.3	38.2	-5.9	-0.83	-0.05	0.36
	2×4	36.1	-64.8	9.1	0.53	0.20	-0.01
	2×5	-13.8	26.7	-3.2	1.84	-0.10	-1.34
P3R-003	2×3	-23.2	-25.3	-1.4	0.10	-0.38	2.30
	2×4	36.9	-15.7	1.5	0.03	-0.19	-0.90
	2×5	-13.6	41.0	-0.15	0.55	0.26	-1.86
P3R-004	2×3	-29.9	-39.3	6.1	1.19	-0.31	-0.47
	2×4	36.0	48.0	-14.3	0.15	0.04	-0.77
	2×5	-6.1	-8.6	8.2	-0.14	0.09	-2.43
P3R-005	2×3	-34.3	-50.1	-5.4	-0.86	0.91	-1.00
	2×4	42.2	26.7	8.4	-0.29	-0.33	-2.81
	2×5	-7.9	23.4	-3.0	2.46	-0.13	-1.08
P3R-012	2×3	-0.4	-87.0	0.22	-1.01	0.43	-1.32
	2×4	9.7	31.9	-3.1	0.86	0.10	0.28
	2×5	-9.2	55.1	2.9	1.64	-0.21	1.67
P3R-013	2×3	-13.4	1.5	1.3	-0.15	0.35	-0.42
	2×4	17.7	-24.5	-4.9	-0.15	0.14	-1.19
	2×5	-4.3	23.0	3.6	1.57	-0.21	-0.18
P3R-015	2×3	-183.0	27.0	-3.3	-0.71	-0.20	-1.51
	2×4	326.4	0.8	6.6	-0.36	0.05	-4.28
	2×5	-143.5	-27.7	-3.2	1.12	0.04	-1.52
P3R-017	2×3	-10.3	11.6	0.5	0.35	0.24	-0.57
	2×4	7.3	-8.0	-2.4	0.04	0.01	-1.94
	2×5	3.0	-3.6	1.9	0.42	-0.10	-0.12
P3R-018	2×3	18.9	-38.9	-5.0	-0.14	0.69	-1.19
	2×4	-32.3	-5.7	8.4	-0.17	0.03	5.02
	2×5	13.4	44.6	-3.4	1.19	-0.27	-2.17
P3R-021	2×3	-37.1	-70.2	1.5	0.67	-0.53	-3.03
	2×4	44.8	19.8	-6.9	0.47	-0.10	-2.34
	2×5	-7.7	50.4	5.4	1.05	0.25	-0.75

panel	sensor	R_x (μm)	R_y (μm)	R_z (μm)	Ω_x (mrad)	Ω_y (mrad)	Ω_z (mrad)
P3R-022	2×3	-36.3	-29.1	-0.2	-0.05	0.29	-0.49
	2×4	38.9	58.5	-1.3	0.10	-0.09	-2.54
	2×5	-2.5	-29.5	1.5	0.95	-0.05	-2.52
P3R-024	2×3	3.8	7.7	1.4	-0.08	0.00	1.01
	2×4	-1.0	-51.3	-4.6	0.45	-0.01	2.16
	2×5	-2.8	43.6	3.2	0.66	0.00	-1.16
P3R-028	2×3	-27.9	-11.2	-1.0	1.20	-0.38	-1.99
	2×4	29.4	5.6	-1.7	0.39	-0.32	-0.86
	2×5	-1.5	5.7	2.7	0.44	0.33	-1.92
P3R-042	2×3	-16.5	-65.8	-8.7	-0.24	0.49	3.91
	2×4	29.1	-18.7	11.2	1.30	-0.27	-1.88
	2×5	-12.6	84.5	-2.5	2.44	-0.02	-1.23
P3R-045	2×3	-13.7	-99.8	-15.9	-0.014	-0.03	-0.68
	2×4	48.8	184.2	31.5	-0.49	0.90	5.80
	2×5	-35.1	-84.4	-15.6	0.64	-0.54	-0.85
P3R-047	2×3	-31.3	36.2	1.1	-0.17	0.52	-1.42
	2×4	40.7	-25.2	-4.1	0.01	0.15	-3.05
	2×5	-9.4	-11.0	3.0	1.22	-0.28	-0.07
P3R-048	2×3	6.7	-74.1	-5.3	0.28	0.27	-1.47
	2×4	-1.1	31.2	7.3	0.18	-0.12	1.91
	2×5	-5.6	42.8	-2.0	1.37	-0.02	1.08
P3R-065	2×3	3.0	-27.5	-3.3	-0.39	1.38	-1.34
	2×4	-35.7	26.9	3.2	0.47	-0.11	-1.56
	2×5	32.7	0.5	0.2	1.89	-0.44	-2.21
P3R-073	2×3	-36.7	0.9	12.4	-0.48	0.39	-11.8
	2×4	21.9	-9.4	-26.5	-0.53	0.17	0.07
	2×5	14.8	8.5	14.0	1.89	-0.25	-0.87
P3R-074	2×3	-9.8	13.5	-1.3	-0.22	0.42	-0.30
	2×4	10.3	-6.0	0.5	0.00	0.33	-0.34
	2×5	-0.5	-7.5	0.8	1.37	-0.36	-0.87
P4L-001	1×2	101.5	-26.1	-7.7	0.58	-3.29	0.10
	2×3	-97.8	-31.1	0.3	0.27	0.89	4.64
	2×4	-129.3	-45.3	22.8	-0.29	0.51	-0.09
	1×5	125.7	102.6	-15.5	-2.16	0.17	0.14
P4L-003	1×2	30.0	-74.2	-24.4	1.40	-0.12	2.14
	2×3	-18.5	41.8	23.8	-0.48	0.88	2.18
	2×4	-80.1	20.7	23.7	-0.31	0.11	2.03
	1×5	68.5	11.8	-23.1	-1.62	-0.31	-0.05

panel	sensor	R_x (μm)	R_y (μm)	R_z (μm)	Ω_x (mrad)	Ω_y (mrad)	Ω_z (mrad)
P4L-004	1×2	60.9	-102.7	-34.6	-0.18	0.56	-0.11
	2×3	-70.2	52.8	42.1	0.50	-4.91	4.82
	2×4	-69.1	48.2	19.2	0.22	0.59	0.64
	1×5	78.4	1.8	-26.7	-1.63	1.04	0.61
P4L-005	1×2	22.1	-43.3	-3.1	0.40	-0.95	-2.71
	2×3	-9.4	-26.4	6.9	-0.61	0.15	2.44
	2×4	-61.8	-47.3	-7.3	-0.25	-0.05	0.56
	1×5	49.13	117.1	3.5	-1.21	0.20	0.51
P4L-006	1×2	22.3	54.1	12.5	1.43	1.32	-6.91
	2×3	-19.9	-96.7	-22.3	-1.45	0.18	2.42
	2×4	-45.3	61.3	5.6	-0.07	-0.21	2.8
	1×5	42.8	-18.7	4.2	-0.77	-0.24	0.41
P4L-007	1×2	30.0	-69.0	-18.7	-0.31	-0.76	0.60
	2×3	-28.5	5.4	11.1	-0.40	0.47	2.31
	2×4	-68.2	-13.9	32.6	-0.27	-0.18	1.39
	1×5	66.7	77.5	-24.9	-2.77	0.14	2.21
P4L-008	1×2	-3.2	-74.8	-13.3	-0.09	-0.16	0.04
	2×3	24.0	9.6	-5.6	-0.84	1.32	3.79
	2×4	-69.4	4.5	50.9	-0.57	-3.29	1.35
	1×5	48.6	60.7	-32.0	-0.65	1.63	0.49
P4L-010	1×2	7.8	-78.2	-16.4	0.13	-0.45	3.83
	2×3	13.2	32.9	15.0	-0.67	0.50	3.94
	2×4	-112.3	-74.5	16.2	-0.55	-0.03	4.67
	1×5	91.3	119.7	-14.8	-1.55	-0.03	0.96
P4L-011	1×2	-13.4	-62.6	-10.6	-0.03	-0.21	-1.06
	2×3	11.7	-1.04	8.6	0.27	0.08	1.96
	2×4	-10.8	29.6	13.1	-0.63	-0.36	2.30
	1×5	12.6	34.0	-11.0	-2.98	0.24	1.06
P4L-012	1×2	76.9	-87.2	-9.9	0.93	-0.14	5.57
	2×3	-79.5	-77.9	9.9	0.05	0.33	2.26
	2×4	-93.3	8.0	7.2	-0.79	0.15	2.04
	1×5	95.9	157.1	-7.1	-3.61	-0.16	-1.41
P4L-014	1×2	32.2	-63.6	-10.1	0.81	-0.79	0.56
	2×3	-56.2	-22.5	7.1	0.17	0.56	4.62
	2×4	-15.3	-8.6	14.5	-0.81	0.18	1.46
	1×5	39.3	94.7	-11.5	-2.61	-0.10	0.79
P4L-015	1×2	29.4	-153.7	3.0	2.07	3.83	3.42
	2×3	-51.9	-22.5	5.6	-0.75	4.16	3.31
	2×4	-45.5	-20.4	-25.9	-0.93	3.18	2.47
	1×5	68.0	196.6	17.3	-3.15	-4.13	4.16

panel	sensor	R_x (μm)	R_y (μm)	R_z (μm)	Ω_x (mrad)	Ω_y (mrad)	Ω_z (mrad)
P4L-017	1×2	15.7	-91.2	-49.5	7.65	-0.46	-1.00
	2×3	53.5	2.2	45.0	2.41	-0.19	0.10
	2×4	-149.6	-55.4	58.5	-2.34	-0.29	-0.39
	1×5	80.4	144.5	-54.0	-6.68	0.35	-1.68
P4L-037	1×2	-1.1	-39.8	14.5	-0.30	2.22	0.76
	2×3	13.3	-50.1	-13.7	-0.90	1.69	-1.29
	2×4	8.2	-37.4	-21.1	-0.69	1.93	-2.64
	1×5	-20.4	127.4	20.3	-3.35	-2.22	-1.85
P4R-001	1×2	11.5	132.1	-20.5	1.32	-0.67	-1.67
	2×3	-31.0	17.3	21.6	0.25	-0.38	-0.57
	2×4	91.2	-46.1	15.7	-1.19	0.01	-2.14
	1×5	-71.7	-103.3	-16.8	-1.91	0.27	-5.94
P4R-004	1×2	-33.0	-49.6	-11.2	1.92	0.59	-1.45
	2×3	22.1	11.1	10.8	0.44	0.046	0.34
	2×4	48.9	-38.4	12.5	-0.29	-0.12	0.60
	1×5	-37.9	76.8	-12.1	-0.97	-0.08	0.75
P4R-005	1×2	-84.2	73.6	-40.3	2.91	0.38	-0.93
	2×3	103.7	120.1	32.4	1.36	0.08	3.66
	2×4	27.7	-125.9	56.7	-1.13	0.32	0.95
	1×5	-47.2	-67.7	-48.7	-5.06	-0.31	-0.74
P4R-011	1×2	-5.9	-49.0	-16.3	1.22	0.16	1.90
	2×3	1.8	-20.7	12.8	0.36	-0.04	-0.57
	2×4	14.79	9.0	24.0	-0.33	0.28	-0.17
	1×5	-10.8	60.7	-20.4	-1.18	-0.20	-0.04
P4R-020	1×2	-92.9	-23.9	-30.2	1.19	0.56	0.81
	2×3	68.2	34.3	40.7	0.77	-1.74	7.16
	2×4	108.9	6.7	8.2	-0.20	0.31	-0.17
	1×5	-84.2	-17.0	-18.7	-1.86	0.22	0.98
P4R-022	1×2	-40.4	-21.3	2.3	6.51	0.23	0.73
	2×3	59.8	-29.9	-18.4	0.64	-0.32	6.13
	2×4	-6.5	-2.2	35.2	0.46	-0.18	-2.18
	1×5	-12.8	53.4	-19.1	-3.45	0.15	-1.18
P4R-024	1×2	-65.1	-27.4	2.9	0.17	-0.39	-2.84
	2×3	90.0	-48.7	0.3	-1.03	-0.11	-1.07
	2×4	47.1	-28.5	-15.6	-0.61	1.20	-2.24
	1×5	-71.9	104.7	12.4	-5.81	-0.61	-1.72
P4R-028	1×2	53.5	18.4	-33.7	1.38	0.66	2.47
	2×3	-104.3	-49.4	41.1	1.81	0.74	-0.08
	2×4	45.1	-58.7	19.7	-0.46	0.07	-0.57
	1×5	5.7	89.7	-27.1	-2.88	-0.42	1.49

panel	sensor	R_x (μm)	R_y (μm)	R_z (μm)	Ω_x (mrad)	Ω_y (mrad)	Ω_z (mrad)
P4R-029	1×2	1.3	-0.3	-24.2	3.00	-0.04	-2.43
	2×3	-5.3	-66.5	24.4	0.52	-0.38	-1.43
	2×4	36.1	-75.4	24.6	-0.11	0.05	-0.66
	1×5	-32.0	142.2	-24.8	-2.03	0.10	-2.00
P4R-030	1×2	-31.5	-25.0	-18.6	1.37	-0.12	4.43
	2×3	33.0	-102.1	15.2	0.25	-0.15	0.23
	2×4	-18.7	-29.5	23.8	-0.97	0.14	1.83
	1×5	17.2	156.6	-20.4	-2.49	-0.01	3.79
P4R-033	1×2	-34.4	10.5	-10.0	-0.34	0.20	-1.44
	2×3	44.7	-57.5	-0.0	-0.04	0.09	-0.86
	2×4	11.6	-9.6	29.0	-0.47	0.11	0.45
	1×5	-21.8	56.5	-19.1	-3.25	-0.14	0.58
P4R-036	1×2	-41.8	53.1	-2.5	0.10	-0.15	-0.30
	2×3	48.2	-23.1	2.6	-0.07	1.05	-0.07
	2×4	56.5	-65.7	-0.9	-0.63	1.39	-2.28
	1×5	-63.0	35.7	0.7	-3.84	-1.14	-1.95
P4R-038	1×2	-66.7	-88.1	-2.3	-1.82	-0.39	-1.12
	2×3	99.0	-25.7	0.6	0.55	0.15	0.40
	2×4	11.5	-61.9	6.0	-0.05	0.036	-0.66
	1×5	-43.8	175.8	-4.2	-1.67	0.02	-1.44
P4R-043	1×2	-25.8	22.5	-14.1	1.25	0.96	1.40
	2×3	24.8	-53.6	5.3	0.45	0.37	0.18
	2×4	40.1	-70.5	33.3	-0.20	0.36	-0.46
	1×5	-39.1	101.6	-24.5	-1.54	-0.56	-1.81
P4R-048	1×2	-2.5	-57.0	-2.8	0.08	0.84	-1.34
	2×3	9.2	-117.5	5.0	-0.41	0.70	-1.31
	2×4	10.2	-44.4	-5.3	-0.69	1.05	-0.49
	1×5	-16.9	218.9	3.1	-2.75	-1.05	-1.58
P4R-059	1×2	1.8	-27.0	-4.8	2.13	1.05	-1.11
	2×3	14.8	-44.6	-10.1	0.56	0.03	-1.59
	2×4	-26.2	-28.8	37.9	0.08	-0.20	-1.02
	1×5	9.6	100.3	-23.0	-2.13	-0.13	0.48
P4R-066	1×2	-11.4	2.9	-20.4	1.31	0.39	0.71
	2×3	20.7	-13.3	23.1	0.90	-0.22	2.12
	2×4	-0.5	-37.8	13.7	-1.42	-0.05	-2.01
	1×5	-8.8	48.1	-16.3	-0.49	0.01	-0.86

panel	sensor	R_x (μm)	R_y (μm)	R_z (μm)	Ω_x (mrad)	Ω_y (mrad)	Ω_z (mrad)
X0004	1×2	-32.3	-49.0	-19.7	3.49	0.94	-1.50
	2×3	22.4	11.3	21.2	0.47	0.36	0.26
	2×4	46.6	-39.3	16.6	-0.76	0.12	0.59
	1×5	-36.7	76.9	-18.1	-1.03	-0.40	0.71
A01L	2×3	-45.6	-91.4	-1.6	0.45	0.25	4.75
	2×4	143.4	-89.4	-0.2	0.03	0.22	-3.40
	2×5	-97.8	180.8	1.8	-2.37	-0.23	-7.12
A02	2×3	-10.5	49.1	-7.0	1.06	-0.12	0.87
	2×4	27.6	-116.9	12.5	0.24	-0.61	0.95
	2×5	-17.2	67.8	-5.4	-2.21	0.42	-2.03
XA01	2×3	-10.5	17.0	0.4	0.96	-0.67	-1.99
	2×4	28.3	-28.5	-1.0	-0.12	-0.35	0.35
	2×5	-17.8	11.5	0.7	-1.00	0.46	-0.19

A.2 Panel Visualization (first 25 production panels)

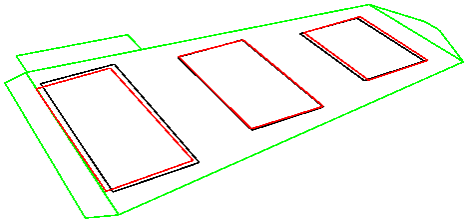

Figure 26: P3R-001

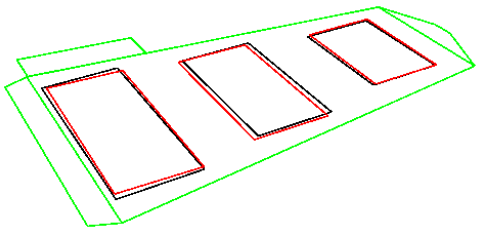

Figure 27: P3R-002

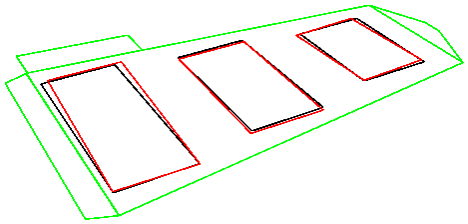

Figure 28: P3R-003

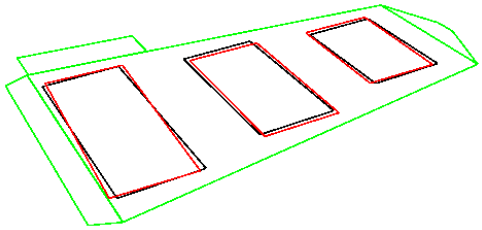

Figure 29: P3R-004

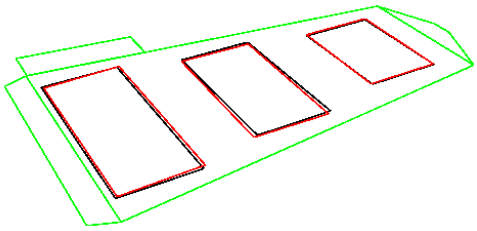

Figure 30: P3R-013

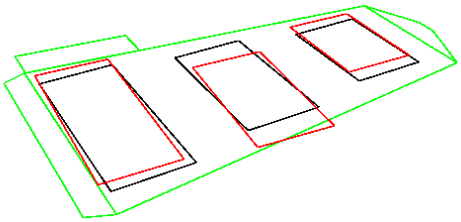

Figure 31: P3R-015

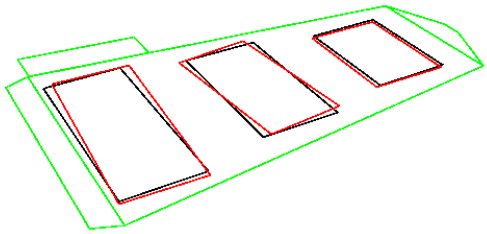

Figure 32: P3R-018

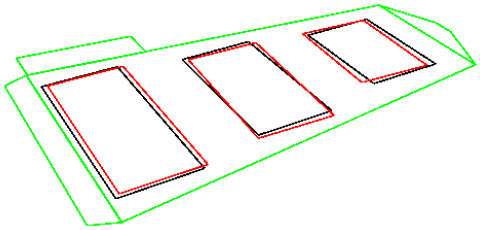

Figure 33: P3R-021

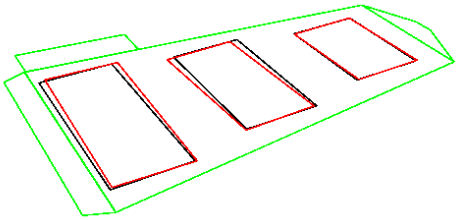

Figure 34: P3R-024

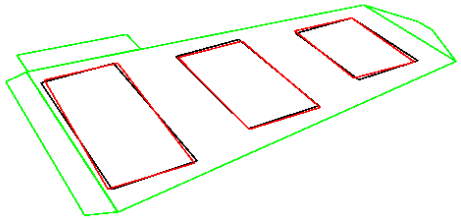

Figure 35: P3R-028

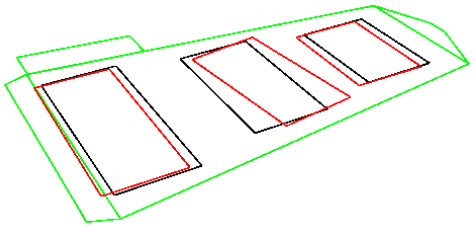

Figure 36: P3R-045

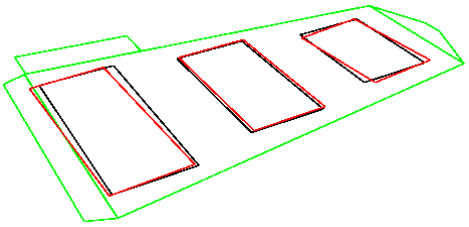

Figure 37: P3L-002

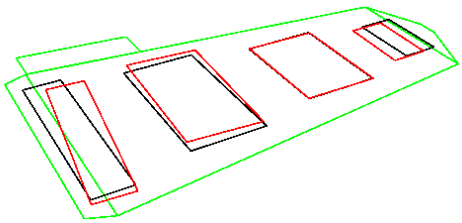

Figure 38: P4R-001

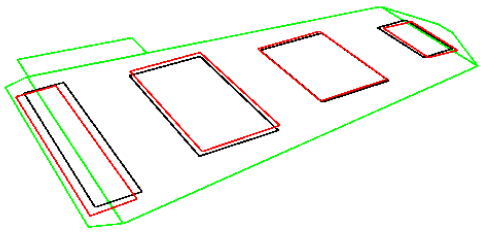

Figure 39: P4R-004

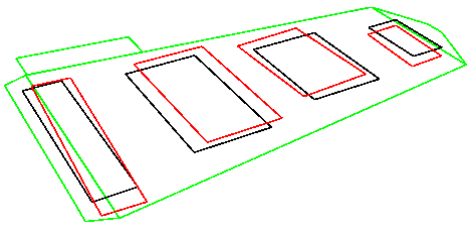

Figure 40: P4R-005

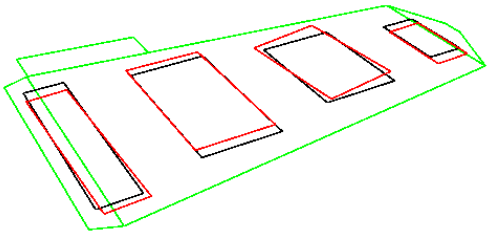

Figure 41: P4R-020

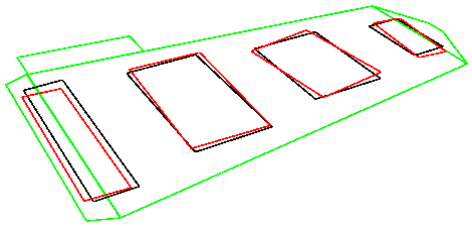

Figure 42: P4R-022

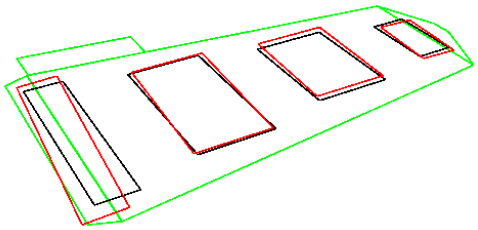

Figure 43: P4R-024

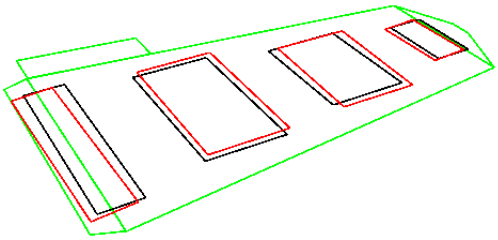

Figure 44: P4R-028

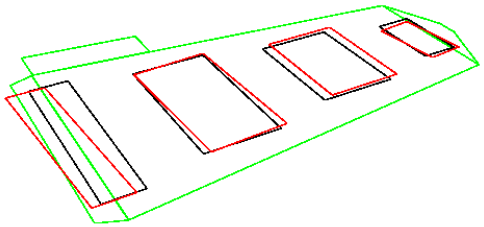

Figure 45: P4R-030

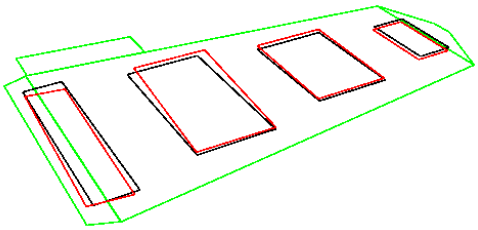

Figure 46: P4R-036

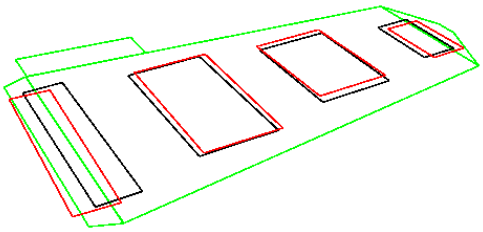

Figure 47: P4R-038

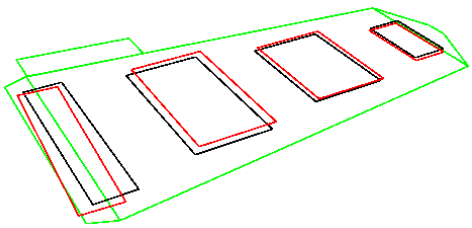

Figure 48: P4R-043

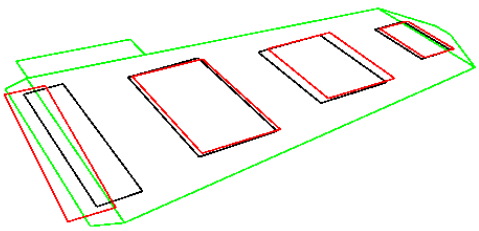

Figure 49: P4R-048

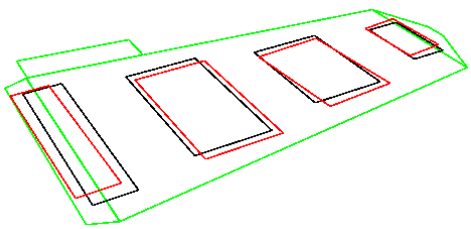

Figure 50: P4L-001

B Database Information

Our current analysis is run by reading in text files of survey data compiled on the PPDserver at fermilab which have been modified for our use. This includes surveys of panels, half disks, and survey balls. Currently, there is data for 30 production panels and 5 prototype panels. Optical survey of the half disk and survey ball measurements are still in the early stages, but we have been using preimlinary measruements. In addition, from our analysis, we have created a database of sensor displacements on a panel, panel displacements on the half disk, and half disk displacements on the full half disk. Thus, the information from survey that will be put in the database is divided into two types, "raw data" and "analysis data".

B.1 Raw Data

For the raw panel survey data, we have been using data of this format:

Panel SN	Plaquette SN	ROC	Fiducial	x_{mes}	y_{mes}	z_{mes}

- **Panel SN** - Gives the serial number of the panel to link with half disk survey
- **Plaquette SN** - Gives the plaquette serial number to link to each panel
- **ROC and Fiducial** - A convention we develop to label each possible fiducial point for each possible sensor. ROC convention is given below. The Fiducial paramter ranges from 1-20 and the number is given in [1].

1×2:

1	2

2×3:

5	4	3
0	1	2

2×4:

7	6	5	4
0	1	2	3

2×5:

9	8	7	6	5
0	1	2	3	4

1×5:

0	1	2	3	4

- x_{mes}**,** y_{mes}**,** z_{mes} - These are the positions of those fiducial points measured during optical survey.

For the half disk survey data, we have been using data of this format:

Reference Target	Reference Target Weight	x_{ref}	y_{ref}	z_{ref}

Panel Name	Panel Position	Panel Type	Sensor	ROC	Fiducial	x_{mes}	y_{mes}	z_{mes}

- **Survey Ball Name** - This is the name of the survey ball (totalling 5) that would agree with the values from the raw data for survey ball positions (below). This is used to relate the survey balls from each set of raw data.
- **Survey Ball Weight** - This tells whether or not we use this ball in joining the two sides (some balls are unstable and thus unreliable).
- x_{mes}**,** y_{mes}**,** z_{mes} - These are the positions of those fiducial points measured during optical survey.
- **Panel Name** - Same as above.
- **Panel Position** - Ranges from 1-12; this is the position of the panel on the half disk.
- **Panel Type** - Same as above.
- **Sensor** - Same as above.

- **ROC and Fiducial** - Same as above.
- x_{mes}, y_{mes}, z_{mes} - Measured points in optical survey.

For the survey ball position data, we have been using data of this format:

Survey Ball Name	x_{mes}	y_{mes}	z_{mes}

- **Survey Ball Name**- The name given to the ball from survey.
- x_{mes}, y_{mes}, z_{mes} - Same as above.

B.2 Analysis Data

The content and format of analysis data is given in tables thorought this note. For sensor analysis data, refer to Table 5. For panel analysis data, refer to Table 1. For half disk analysis data, refer to Table 3.

References

[1] G. Bolla, "Alignment marks on sensor for post plaquette assembly survey and positioning," FNAL DOCDB Note CMSpix-doc-406 (2005), see https://docdb.fnal.gov/

[2] For an example of survey data, see G. Derylo, "Panel CMM Survey Sample Data" FNAL DOCDB Note CMSpix-doc-1082 (2006).

[3] G. Derylo, "Panel Mechanical Assembly Procedures," item 12 "OGP Survey of Sensor Locations," FNAL DOCDB Note CMSpix-doc-424 (2006).

[4] R. Brun *et al.*, "Root data-analysis framework", http://root.cern.ch/

[5] V. Chiochia, "Proposed New Coordinate Frames for FPIX Goemetry," http://www.uscms.org/LPC/lpc_simul/activities/FPiX/sensorLocalFrames.pdf

[6] M. Kubantsev, "Development of Survey of the Elements of Half Disk of the CMS Forward Pixels," FNAL DOCDB Note CMSpix-doc-1222-v2 (2006).

[7] P. Schleper, G. Steinbrueck, M. Stoye, "Software Alignment of the CMS Tracker using MILLEPEDE II," CMS NOTE-2006/011; V.Karimaki, T.Lampen, F.-P.Schilling, "The HIP Algorithm for Track Based Alignment and its Application to the CMS Pixel Detector," CMS NOTE-2006/018; E. Widl, R. Fruehwirth, W. Adam , "A Kalman Filter for Track-based Alignment," CMS NOTE-2006/022.

[8] A. V. Gritsan, C. K. Lae, N. Tran, note in preparation.

[9] D. N. Brown, A. V. Gritsan, D. A. Roberts, "Local Alignment of the BABAR Silicon Vertex Tracker," BABAR Analysis Document 486, to be published.

[10] A. V. Gritsan, M. Kubantsev, and N. Tran, "Application of the Optical Survey to the Pixel Software Alignment," Presentation at CMS Pixel Software Meeting July 12, 2006, FNAL DOCDB Note CMSpix-doc-1119 (2006).